FINAL TECHNICAL REPORT

Probabilistic Residual Shear Strength Criteria for Post-Liquefaction Evaluation of Cohesionless Soil Deposits

USGS Grant Number: 04HQGR0076

M. Gutierrez, M. Eddy and P.M.H. Lumbantoruan
Civil and Environmental Engineering
Virginia Polytechnic Institute & State University
200 Patton Hall, Blacksburg, VA 24061

NEHRP Element: PT

Research supported by the U.S. Geological Survey (USGS), Department of the Interior, under USGS award number: M. Gutierrez 04HQGR0076. The views and conclusions contained in this document are those of the authors and should not be interpreted as necessarily representing the official policies, either expressed or implied, of the U.S. Government.

Corresponding address:
Marte Gutierrez, PhD
Civil and Environmental Engineering
Virginia Polytechnic Institute and State University
200 Patton Hall, Blacksburg, VA 24061
Tel: 540-231-6357, Fax: 540-231-7532
E-mail: magutier@vt.edu

NON-TECHNICAL SUMMARY

Liquefaction is the phenomena where cohesionless soils lose strength as a result of excessive earthquake shaking, static loads, or deformations. Over the past 40 years, engineers have documented hundreds of failures where liquefaction was the apparent culprit. Researchers have made attempts to determine the strength of susceptible material before and after liquefaction has occurred based on these cases. However, the analyses have not directly accounted for the variability of material properties. The main objectives of this research project are to quantify uncertainties associated with the various case histories and provide procedures for analyzing liquefiable soil deposits and their post-liquefied shear strengths within a risk-based framework.

Key Words:

Liquefaction, Flow Failure, Liquefied Shear Strength, Probability, Reliability

ABSTRACT

The main objective of the research presented in this report is to develop improved procedures for determining the post-liquefaction shear strength of cohesionless soils from in situ tests. The residual or liquefied shear strength is the main factor determining the post-liquefaction stability of embankment dams and foundations, and whether a soil mass will experience flow failure or significant deformations. The cost and extent of measures required to ensure the stability of embankment dams against liquefaction are greatly influenced by the magnitude of the liquefied shear strength. As pointed out by Seed (1987), it may be adequate and economically advantageous simply to ensure the stability of an earth deposit or structure against flow failure after the strength loss has been triggered than to prevent the triggering itself.

One method to determine the liquefied shear strength is the use of case histories where the liquefied shear strength is back calculated from case studies of liquefaction in soil zones where penetration test results were available. However, the case-histories approach has several limitations including the very limited amount of data from field case histories, the significant uncertainties involved in the back-calculation of the liquefied shear strengths, and the lack of consistent and rational methods to use the available data on liquefied shear strength of granular soils.

In order to address the current limitations in evaluating the post-liquefaction evaluation of cohesionless soil deposits using in situ tests, the project aims to: 1) re-evaluate and expand the available database on liquefied shear strengths of liquefied soils, 2) clearly delineate and systematically analyze the magnitudes of uncertainties involved in evaluating post-liquefaction shear strength, 3) develop robust, reliability-based procedures for back-calculating the liquefied

shear strength from case histories, and 4) develop new probabilistic procedures for evaluating the liquefied shear strength for post-liquefaction stability analysis of embankment dams.

Based on a literature review, previously studied and new cases of flow liquefaction were identified and critically reviewed before they are included in a database of post-liquefaction case histories. Using a First-Order-Reliability-Method (FORM), Monte-Carlo Simulation (MCS), and Bayesian Mapping (BM), reliability-based back-analysis procedures were developed to provide rigorous methods for determining liquefied shear strengths from case histories and quantifying their reliability.

Uncertainties in parameters needed to establish the liquefied shear strengths and the SPT-values were quantified and used to determine the reliability of the field data. Using the database of reliability indices of the field data, probabilistic post-liquefaction shear strength criteria were formulated to provide measures of risk in terms of probability of failure, which could be used in conjunction with traditional factors of safety.

The figure below shows the proposed probabilistic liquefaction criteria in terms of the liquefied shear strength S_{u-LIQ} vs. the minimum SPT blow count $(N_1)_{60}$ (uncorrected for fines content). The average $S_{u\text{-}LIQ}$ vs. $(N_1)_{60}$ is equal to:

$$S_{U-LIQ} = 0.87 \min(N_1)_{60} + 0.1(\min(N_1)_{60})^2$$

The curves corresponding to probabilities of failure (P_F) equal to 2%, 16%, and 50% for flow failure demand (*FFD*) or the value of shear stress necessary to produce that particular probability of failure are shown in the figure. The specific equations for the FFD vs. $(N_1)_{60}$ for the different probabilities of failure are given below:

For P_F = 2%:

$$S_{U-LIQ} = \left(\frac{1}{4}\right)\left[0.87\min(N_1)_{60} + 0.1(\min(N_1)_{60})^2\right]$$

For P_F = 16%:

$$S_{U-LIQ} = \left(\frac{1}{1.85}\right)\left[0.87\min(N_1)_{60} + 0.1(\min(N_1)_{60})^2\right]$$

For P_F = 50%:

$$S_{U-LIQ} = \left(\frac{1}{1.048}\right)\left[0.87\min(N_1)_{60} + 0.1(\min(N_1)_{60})^2\right]$$

The probabilistic criteria will provide engineers and geologists with tools to make better decisions on devising measures to mitigate liquefaction or to reduce the uncertainty in the evaluation of the liquefaction potential of earth dams and sites.

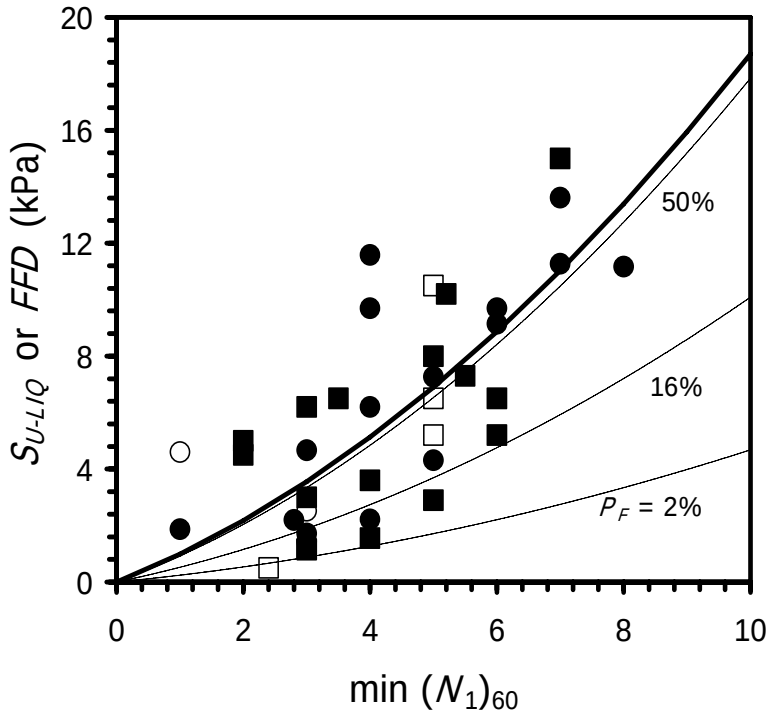

Contours of probability of failure P_F computed with the liquefied shear strength vs. SPT blow count relation

TABLE OF CONTENTS

CHAPTER 1 - SIGNIFICANCE AND BACKGROUND OF RESEARCH

When earthquakes occur, the resulting death and destruction can be widespread and unforgiving. Common examples of earthquake-induced damage include complete structural collapse, tilting or overturning of buildings, and flow failure of earth dams and slopes. Liquefaction, a phenomenon where loose soil deposits lose considerable shear strength during earthquakes, is considered to be one of the primary causes of earthquake-related damage. When structures are constructed atop or of liquefiable materials the consequences can be disastrous.

Seed (1987) points out two important issues related to the liquefaction of soils: 1) the stress conditions that trigger liquefaction, and 2) the consequences resulting from the liquefaction. With the first issue, determining the triggering stress conditions provides insight into whether or not the soil will liquefy. This topic is comprehensively discussed by Youd et al. (2001). Addressing the second issue requires estimation of the available shear strength after liquefaction has occurred. Early studies on the shear strength of granular soils by Castro (1969) showed that after liquefaction, granular soils can retain significant resistance to shear deformation. Different terms have been used to refer to the post-liquefaction resistance including:

- *Residual shear strength* (Seed, 1987)
- *Residual undrained shear strength* (Seed and Harder, 1990)
- *Undrained steady state shear strength* (Poulos et al., 1985)
- *Quasi-steady state shear strength* (Ishihara, 1993)
- *Critical shear strength* (Stark and Mesri, 1992)
- *Liquefied shear strength* (Stark et al., 1997)

The term *liquefied shear strength*, $S_{u\text{-}LIQ}$, will be used to describe the undrained post-liquefaction shear strength in this proposal.

Seed (1987) states that it may be economically advantageous to simply ensure the stability of an earth deposit or structure against post-liquefaction failure rather than prevent triggering itself. It is now increasingly being recognized that determination of the liquefied shear strength could be more important than determination of the stress conditions that trigger the liquefaction itself (e.g., Ishihara, 1993; Stark et al., 1997; Finn, 2000). The liquefied shear strength is the main factor when determining whether a soil mass will experience flow failure or large deformations due to earthquake or static loading. The cost and extent of remedial measures required to mitigate the liquefaction of soil deposits are, therefore, greatly influenced by the magnitude of the liquefied shear strength. The liquefied shear strength can be used in slope stability analyses or other numerical models to provide a simple and attractive means for estimating potential instabilities and/or deformations of liquefiable soil deposits.

Over the past forty to fifty years, the subject of liquefaction has received considerable attention through documentation of case failures and extensive laboratory testing. There are currently two methods for estimating the liquefied shear strength of soil deposits. One approach for determining the liquefied shear strength is the *laboratory procedure*. Poulos et al. (1985) developed a procedure for assessing flow liquefaction using the results of monotonically loaded, consolidated-undrained triaxial tests. While laboratory testing programs have contributed a tremendous wealth of information regarding the liquefied shear strength of soils, disturbance during sampling hinders the use of these strengths in subsequent analyses on actual projects. Although it is possible to use reconstituted soil samples, it is usually difficult to accurately determine in-situ void ratios. More importantly, the costs of sampling and laboratory testing are

generally prohibitive on typical projects. The other method is the *case histories approach* where the liquefied shear strength is back-calculated from case histories of liquefaction instability in soil zones where in-situ testing parameters were measured or can be estimated. The shear strength is computed by analyzing the failure conditions using traditional limit equilibrium slope stability models. Databases of case histories for flow liquefaction have been developed by Seed (1987), Seed and Harder (1990), Stark and Mesri (1992), Ishihara et al. (1990a, 1993), Castro (1995), and Olson and Stark (2003).

Although the use of field data and case histories should be preferred, there are several limitations with regards to the case histories approach. These limitations are:

1. There is a limited amount of data on back-calculated liquefied shear strengths from field case histories,
2. All available procedures for estimating the liquefied shear strength are based on deterministic methods and do not directly account for parameter uncertainties, and
3. There is currently a lack of consistent and rational methods to use the available data on liquefied shear strength of soil deposits for analyzing sloping ground.

In addition, there are several un-resolved differences in opinion and disagreements on the interpretation and use of the liquefied shear strength data from field case histories, including whether the liquefied shear strength should be normalized with respect to the initial effective vertical stress, and whether to correct the in-situ test parameters for fines content.

CHAPTER 2 - PROJECT OBJECTIVES

This research project aims to quantify uncertainties associated with the post-liquefaction residual shear strength of cohesionless soil deposits. The primary goal of this research is to develop robust, reliability-based procedures for determining the liquefied shear strength of cohesionless soils based on the back analysis of historical flow liquefaction. These failures will be obtained from existing databases and additional cases will be sought out from the available literature to create a comprehensive database. Results from these analyses should also provide insight into two controversial questions:

1. Should the liquefied shear strengths be normalized by the initial effective vertical stress?
2. Should in-situ test parameters such as the SPT blow count be corrected for fines content?

The main objectives of the current research project are to quantify the uncertainties involved in available case histories of liquefaction failure using probabilistic techniques and to provide improved procedures for estimating the liquefied shear strength of susceptible soil deposits from in-situ test parameters. The following list gives the specific objectives to be addressed in this research project:

1. Re-evaluate and expand the available databases of flow liquefaction case histories where SPT data or other in-situ data are available,
2. Cleary delineate and systematically analyze the magnitudes of uncertainties involved in evaluating the liquefied shear strength from case histories,
3. Develop robust, reliability-based procedures for back-calculating the liquefied shear strength from case histories, and
4. Develop new probabilistic liquefied shear strength criteria for liquefiable soils based on in-situ test data.

This report is subdivided into five chapters to provide discussion on different aspects of the research. Chapter 3 deterministically analyzes the different case histories of liquefaction case histories. Included are re-analyses of case histories that have been previously reported in the literature, and analyses of new case histories. Chapter 3 addresses also issues such as correcting for fines content, and normalization of the liquefied shear strength with respect to the initial effective vertical stress. Chapter 4 describes the probabilistic analyses of the case histories presented in Chapter 4. Finally, Chapter 5 summarizes the research, and presents the authors' final conclusions and recommendations for performing probabilistic analyses of sloping ground containing potentially liquefiable cohesionless soils.

CHAPTER 3 - DETERMINISTIC ANALYSIS OF FLOW FAILURE CASES

Summary

The critical parameter involved in assessing and designing against the harmful effects of liquefaction is the liquefied shear strength, or the shear resistance available after liquefaction has occurred. Selection of the liquefied shear strength is an important decision because the chosen value can either unnecessarily drive up construction costs or lead to the construction of unsafe structures. This paper presents deterministic back-calculation procedures to analyze case histories of flow liquefaction. Existing databases are re-considered and re-analyzed, and additional case histories are studied to expand available databases. Regression analyses are then performed to develop new correlations between the liquefied shear strength and Standard Penetration Test (SPT) blow count. Factors affecting the liquefied shear strength determined from field data, such as the effects of fines content and normalization with respect to the initial effective vertical stress, are also discussed. This chapter provides background for the next chapter which presents probabilistic procedures to evaluate liquefied shear strengths from case histories and their correlations to SPT blow count.

Introduction

Liquefaction, a phenomenon where loose soil deposits lose considerable shear strength during earthquakes, is considered to be one of the primary causes of earthquake-related damage. Liquefaction can also occur under static conditions such as during construction. When structures are constructed atop or of liquefiable materials the consequences of liquefaction can be disastrous. When analyzing the stability of liquefiable soil deposits, particularly in determining whether flow liquefaction can occur, the current state-of-the-art entails characterizing the soil

deposit with Standard Penetration Tests (SPT) or with other in situ testing methods and estimating the liquefied shear strengths. Empirical relationships between liquefied shear strengths and SPT blow count have been developed by Seed and Harder (1990), Stark and Mesri (1992), and Olson and Stark (2003) from case histories of liquefaction failures. The liquefied shear strengths are then used to assess sloping ground stability with various techniques such as limit equilibrium, and finite difference and finite element analyses. Selecting appropriate liquefied shear strengths with existing methods, which show significant scatter in the data, can lead to very different results during analysis and design.

The liquefied shear strength is an important parameter when assessing potential slope instability and resulting deformations for liquefiable soil deposits involving sloping ground. The liquefied shear strength is the undrained shear strength remaining after liquefaction has occurred in a soil deposit and is mobilized in the post-failure geometry. As the pore pressures within the soil build-up, the shearing resistance of the soil reduces as liquefaction occurs. The minimum shear strength available following the initial yielding of the soil is the liquefied shear strength. Other terminologies that have been used in the literature to refer to the undrained shear strength that is mobilized after liquefaction has occurred include: *residual shear strength* (Seed 1987), *residual undrained shear strength* (Seed and Harder 1990), *undrained steady state shear strength* (Poulos et al. 1985), *quasi-steady state shear strength* (Ishihara 1993), and *critical shear strength* (Stark and Mesri 1992). Several studies have shown that the liquefied shear strength is the same for both monotonic and cyclic conditions (e.g., Casagrande 1965, Castro 1975, and Ishihara 1993), thus the liquefied shear strength can be used to characterize flow liquefaction potential under both monotonic and cyclic loading conditions.

The main objectives of this chapter are to: 1) re-compile and re-analyze existing cases of flow liquefaction failure, 2) expand existing databases of liquefied shear strength by analyzing new cases of flow liquefaction, and 3) analyze the updated dataset to develop new correlations of the liquefied shear strength with Standard Penetration Test (SPT) blow counts. This chapter presents the methods of back-analysis analysis, case histories and deterministic liquefied shear strength vs. SPT blow count relationships, which will be used to develop probabilistic liquefied shear strength criteria in the next chapter.

Methods of Slope Stability Analysis

Liquefied shear strengths are back-analyzed from case histories of flow liquefaction of natural and engineered slopes using slope stability analyses. Two types of slope stability models are used in the back analysis depending on the post-failure geometrical conditions of the liquefied site. These are: 1) the infinite slope model, and 2) more sophisticated slope stability models utilizing circular or more complicated failure surface geometries.

Many flow liquefaction failures in sloping ground can be analyzed as infinite slopes. Ishihara et al. (1990) used an infinite slope model to estimate the liquefied shear strength of several failures. This study uses a similar infinite slope model to back-calculate $S_{U\text{-}LIQ}$ from the liquefaction failures. If the failure surface is very long then the inter-slice forces must cancel out, the ground surface is parallel to the failure surface, and the phreatic line is also parallel to the ground surface. From equilibrium of forces along the failure surface, the factor of safety *FS* for the infinite slope model under undrained conditions is given by Eqs. (3-1) and (3-2):

$$FS = \frac{S_{u-LIQ}}{\left(W \sin\alpha \cos\alpha\right)} \tag{3-1}$$

$$W = H_d \gamma_m + H_w \gamma_{sat} \tag{3-2}$$

where W is the total weight of the soil above the failure surface, α is the slope of the ground/failure surface measured from the horizontal, H_d is the depth to the water table from the ground surface, H_w is the height of the water table above the failure surface, γ_m is the moist unit weight of the soil above the water table, and γ_{sat} is the saturated unit weight of the soil above the failure surface. This model assumes that the liquefied shear strength $S_{U\text{-}LIQ}$ provides all resistance to sliding under undrained conditions.

Many liquefaction case histories have geometries and slip surfaces requiring analyses more sophisticated than the infinite slope model. These cases require a stability model capable of handling circular and non-circular slip surfaces. Spencer's (1967) generalized method of slices is used to analyze those cases of flow failure where the post-failure geometry is complex. This method satisfies both moment and force equilibrium. The limit equilibrium equations used to solve for the factor of safety FS and inter-slice force inclination θ for Spencer's procedure are presented and discussed in Duncan and Wright (2005). Three important equations are presented here for the case where forces due to seismic loads, surface loads, and reinforcement are ignored (i.e. assuming that all forces act through the center of the base of each slice). To satisfy force equilibrium:

$$\sum Q_i = 0 \tag{3-3}$$

where Q_i is the resultant of interslice forces on slice i assuming that the forces are parallel and act in opposite directions. The summation is performed for i from 1 to the total number of slices. To satisfy moment equilibrium, moments are taken about the origin ($x = 0$, $y = 0$) as shown in Eq. (3-4):

$$\sum Q_i \left(x_{bi} \sin\theta - y_{bi} \cos\theta \right) = 0 \tag{3-4}$$

where x_{bi} and y_{bi} are the *x*- and *y*- coordinates of the center of the base of slice *i*, respectively. Duncan and Wright (2005) show that combining the Mohr-Coulomb failure criterion, and Eqs. (3-3) and (3-4) results in the following equation for the resultant of inter-slice forces:

$$Q_i = \frac{-W_i \sin\alpha_i - \left(c_i' \Delta l_i / FS \right) + \left(W_i \cos\alpha_i + u_i \Delta l_i \right) \left(\tan\phi_i' / FS \right)}{\cos\left(\alpha_i - \theta \right) + \left[\sin\left(\alpha_i - \theta \right) \tan\phi_i' / FS \right]} \tag{3-5}$$

where W_i is the slice weight (function of unit weights in slice *i*, γ_i), α_i is the inclination of the bottom of the slice from the horizontal in degrees, c_i' is the effective cohesion, Δl_i is the length of the base of the slice, u_i is the pore pressure at the center of the base of the slice, and ϕ_i' is the effective friction angle. For undrained conditions c_i' becomes the undrained shear strength S_{ui}, and ϕ_i' is assigned a value of zero. The factor of safety *FS* and the angle θ are changed iteratively until Eqs. (3-3) to (3-5) are satisfied within reasonable levels of error. This iterative procedure can be performed in a spreadsheet using built-in optimization routines like Solver™ in Microsoft Excel™. In the case of back-analysis, the back-calculated parameters are changed such that Eqs. (3-3) to (3-4) are satisfied and *FS* is equal to 1.

The equilibrium equations for the forces acting parallel and normal to the base of the slice are shown in Eqs. (3-6) and (3-7):

$$N + F_v \cos\alpha - F_h \sin\alpha - Q \sin\left(\alpha - \theta \right) = 0 \tag{3-6}$$

$$S + F_v \sin\alpha + F_h \cos\alpha + Q \cos\left(\alpha - \theta \right) = 0 \tag{3-7}$$

where *N* is the normal force acting perpendicular to the base of the slice, *S* is the shear force acting parallel to the base of the slice, F_v is the vertical force acting on the slice and F_h is the horizontal force acting on the slice. F_v and F_h include all external loads including seismic loads,

reinforcing loads, and the weight of the slice. Moments are taken about the origin ($x = 0$, $y = 0$) to satisfy moment equilibrium, resulting in the following equation:

$$\sum Q_i \left(x_{bi} \sin\theta - y_Q \cos\theta \right) = 0 \tag{3-8}$$

Cases of Flow Liquefaction

Existing databases of liquefaction instability failure were re-compiled and re-analyzed, and additional cases from recent earthquakes including the 1993 Kushiro-oki Earthquake, 1993 Hokkaido-Nansei-oki Earthquake, 1995 Hyogoken-Nambu Earthquake, and the 1999 Kocaeli/Izmit Earthquake were included. Table 3-1 presents 38 cases of flow liquefaction failures including the cause of failure and pertinent references that are used in this study. This database includes several failures that have been researched for many years including the 1934 Fort Peck Dam failure where a large flow failure of the upstream slope occurred during dam construction leading to lateral displacements of as much as 460 meters. Another failure, that has always been included in flow failure databases, is the 1918 construction-induced failure of Calaveras Dam, where the failed dam materials traveled nearly 200 meters upstream. The 1971 Lower San Fernando Dam failure involved a flow failure of the upstream shell following the 1971 San Fernando earthquake in southern California. The failure left minimal freeboard preventing a catastrophic overtopping of the dam. Five case histories are included from the recent 1999 Kocaeli/Izmit Earthquake, where numerous flow failures were observed following the earthquake. Three cases were taken from the 1985 Chilean earthquake. Most of the rest of the case histories were taken from sites in Japan.

Most failures are analyzed with a limited number of data making it difficult to accurately locate the sliding surface and to characterize the extent of the liquefied zone, in turn, affecting

the reliability of the back-calculated liquefied shear strengths. The shear strength of non-liquefied soils along the sliding surface also affects the back-calculated liquefied shear strength of the liquefied soils. The limited number of tests, often performed under differing standards, also leads to a difficulty in obtaining SPT or CPT data within or near the surface of sliding. Judgment is required to interpret test results in many of the case histories. For instance, as cited by Olson (2001), eight different experts recommended representative SPT blow counts for the Lower San Fernando Dam failure ranging from 4 to 15. Estimating the location of the phreatic surface during the failure and during the in situ testing are also important factors (Gutierrez et al., 2003).

The post-failure geometries of the failed sites are necessary to estimate the liquefied shear strength. The pre-failure geometry can provide an estimate of the yield shear strength, however, the calculation does not offer an estimate of the shear strength after the soil has liquefied. Post-failure surveys and eyewitnesses accounts provide a means for estimating the post-failure geometry. The cases analyzed in this report were chosen because the post-failure geometries could be reasonably reconstructed for back-calculation of the liquefied shear strength.

The database presented in Table 3.1 has five cases more than the most recent compilation performed by Olson and Stark (2003). Moreover, the current database does not include those cases where the post-failure geometry is indiscernible or difficult to establish, and where only the pre-failure geometry can be constructed. Thus, many of the case histories that are included in this study are different from those reported by Olson and Stark (2003). It should also be noted that of the 33 cases presented by Olson and Stark (2003), 31 cases had insufficient information requiring that some of the parameters had to be estimated to back-calculate the liquefied shear strength. Information necessary to perform slope stability analysis of flow failures include

geometry, zonation of the structures and the soil, location of the water table, and field or laboratory results lending data about the liquefied and non-liquefied materials. Case histories with insufficient data and where reasonable estimates of material properties were not permissible, were left out of the current database. In addition, an attempt was made to choose only cases where SPT blow count data was available. Future studies should develop additional relationships for different in situ tests such as the Cone Penetration Test.

The cases presented in Table 3-1 are analyzed using a combination of infinite slope model and Spencer's generalized method of slices to back calculate the liquefied shear strengths. Table 3-2 and 3-3 present the input parameters for the 38 case histories. Table 3-2 contains parameters for the cases analyzed with the infinite slope model and Table 3-3 contains parameters for the cases analyzed with Spencer's method of slices. For all case histories, the parameters involved in evaluating the liquefied shear strength from field data have been carefully delineated and systematically analyzed.

The flow failures presented in Table 3-1 occurred over a time span of 1907 to 1999, most of which occurred in the second half of the 20th century. This is a result of the drive to document cases of liquefaction failure following the major Japanese and Alaskan earthquakes of the early 1960's. Thirty-three of the 38 failures analyzed were seismically-induced whereas four failed during construction, including Calaveras Dam, Fort Peck Dam, Tar Island Dyke, and the North Dike of Wachusett Dam. One case that is not clearly grouped into either category is the Lake Ackerman Roadway Embankment (Case #18) which failed during a seismic survey where vibratory trucks induced a flow failure of the embankment. Twenty of the 38 cases are analyzed with Spencer's generalized method of slices and the remaining 18 are analyzed with the Infinite Slope model. Sixteen cases of the cases are located in Japan, 10 are located in North America

and the remaining 10 are from South America, Turkey, Eastern Europe, and the old Soviet Union.

For the infinite slope cases, Table 3-2 contains the parameters required to back-calculate the liquefied shear strength including the depth to the water table, the height of water above the failure surface, moist and saturated unit weights, and the inclination of the failure surface. For the Spencer-type cases, Table 3-3 contains the material properties of the non-liquefied soils including friction angles, cohesion, and unit weights. The parameters contained in Tables 3-2 and 3-3 are mean or average values. These values were estimated from previous pre- and post-failure studies of the different case histories.

Back-analysis of Liquefied Shear Strength

The input parameters presented in Table 3-2 for the infinite slope cases, and Table 3-3 for the Spencer-type cases are used to back-calculate the mean or average liquefied shear strength from each case. The slip surface for each of the infinite slope cases is defined by the depth to the water table from the ground surface and the height of water above the failure surface. These values are assessed based on available cross-sections and measurements of the likely zone of liquefied material. For the analysis of the complex cases that cannot be modeled as infinite slopes, the slip surface for each cases was based on re-construction of the post-failure geometry taken from surveys and witness accounts taken after the failure has occurred. In most cases, the reconstructed failure surfaces were verified by parametric slope stability analyses whereby different geometries are tried in conjunction with different values of the liquefied shear strength to obtain a factor of safety of one.

The following steps are followed in locating the failure surface corresponding to post-failure geometries for the non-infinite slope cases: 1) Assign mean input parameters for all zones, 2) Gradually reduce the liquefied shear strength of the failed zone and search for the slip surface that provides a factor of safety of one, and 3) The resulting liquefied shear strength is the back-calculated shear strength. An alternative procedure was also used to determine the slip surface for the post-failure geometry which involved using very low shear strength for the liquefied zone in the order of 0.1 kPa. Using the slip surface obtained for this very low shear strength, the liquefied shear strength is adjusted until a factor of safety of one is obtained. Both procedures result in similar if not the same liquefied shear strengths and slip surfaces for the same cross-section. Analyses using slip surfaces proposed by other researchers based on post-failure geometries were also performed yielding only slight differences in the back-calculated liquefied shear strength.

Table 3-4 lists the back-calculated liquefied shear strengths for the 38 case histories presented in Table 3-1. This table also presents SPT blow counts, fines contents, corrected SPT blow counts, the initial vertical effective stress σ'_{vo}, and the liquefied shear strength ratio S_{u-LIQ}/σ'_{vo}. The SPT blow counts are corrected using several existing methods described below in the section titled "Fines Content." The back-calculated liquefied shear strengths range from 0.5 to 15 kPa with an average of 5.9 kPa. The SPT blow counts reported in Table 3-4 correspond to the minimum SPT blow count. As discussed by Fear and McRoberts (1995), and Wride et al. (1999), the use of average SPT blow counts typically provides conservative values of liquefied shear strength. They also point out that the minimum SPT blow count corresponds to the "weakest-link-in-the-chain" value and is the most likely the factor that leads to liquefaction flow failure.

The liquefied shear strengths presented in Table 3-4 are comparable to data reported in other studies where the post-failure geometry was used such as those presented by Olson and Stark (2003). The presented liquefied shear strengths are lower than those in studies where the pre-failure geometry is used to back-calculate the undrained shear strength (e.g., Seed and Harder, 1990). This is expected as the yield shear strength corresponding to the pre-failure geometry should be higher then the residual shear strength back-calculated from the post-failure geometry. The SPT blow counts presented here are also typically lower than those previously published as they are representative of the minimum blow count.

Regression Analysis of Liquefied Strength Relationships

Least-squares regression analyses are performed on the data presented in Table 3-4 to develop correlations between the liquefied shear strength and SPT blow count that can be used for analysis of liquefied soil deposits and earth embankments. Figure 3-1 presents the best-fit S_{u-LIQ}/σ'_{vo} vs. $(N_1)_{60}$ for the infinite slope cases and the Spencer-type cases using a 2nd order polynomial together with the R^2 values for each of the curves. The best-fit curves for each type of slope stability analysis are very close to each other. While the R^2 value for the infinite slope cases is slightly higher than the R^2 value for the Spencer-type cases, it appears that both types of analyses can be combined in the same liquefied shear strength relationship. All cases presented in Table 3-4 are then used as a single set of data irregardless of the type of analysis in the subsequent regression analyses. The symbols in Figure 3-1 represent the type of stability analysis used for back-analysis and a representation of the SPT quality, namely: squares correspond to cases analyzed with Spencer's method, circles correspond to cases analyzed with the infinite slope model, solid squares or circles indicates that SPT blow counts were measured at the failure

zones, and open squares or circles indicates that the SPT blow counts were estimated from other tests or relative density.

Figure 3-2 presents regression analyses performed on the entire dataset with several different equations including linear, power, logarithmic, exponential, and second-order polynomial equations. Table 3-5 contains the regression equations with the corresponding coefficients, and the R^2 values. The regression equations use SPT blow count not corrected for fines content. Table 3-5 indicates that a 2nd order polynomial provides the best-fit having the highest R^2 value.

In addition to plotting the "best-fit" relation, upper and lower bound curves are plotted to provide a measure of the scatter of the data from the "best-fit" equation. This error is referred to as the standard error of estimate (Spiegel and Stephens, 1999). The standard error of estimate is analogous to the standard deviation when analyzing the spread of data in relation to the mean or average value. The standard error of estimate $S_{Y.X}$ provides a measure of the scatter of the data about the regression line and has an equation of the form:

$$S_{Y.X} = \sqrt{\frac{\sum \left(Y - Y_{est}\right)^2}{N}} \tag{3-9}$$

where Y is the actual liquefied shear strength for a particular blow count Y_{est} is the liquefied shear strength computed with the regression equation, and N is the number of samples. Figure 3-3 contains the "best-fit" second-order polynomial with plus and minus one standard error of estimate. Approximately 71% (27 of 38 cases) of the case histories fall within the one standard error of estimate lines. The upper and lower bound relationships proposed by Seed and Harder (1990) are also plotted on Figure 3-3 for comparison. All 38 cases fall within the upper and lower bounds set by Seed and Harder (1990). The second-order polynomial is roughly parallel to the Seed and Harder (1990) upper bound and is approximately 5 kPa lower on average. It should

be noted that the Seed and Harder (1990) relationship corrects the SPT blow count for fines content as described below, while the SPT values for the data shown in Figure 3-3 are uncorrected for fines content.

Correction for Fines Content

The influence of fines content (*FC*) on liquefaction potential has been studied by numerous researchers. However, there are fewer studies on the effects of fines content on the liquefied shear strength. Studies on the effects of fines content on the liquefaction potential have often yielded conflicting experimental results. For instance, results have shown different effects of non-plastic fines content on the liquefaction resistance of sands, including: 1) little or no effects of fines content on liquefaction resistance (Ishihara 1993), 2) increase in liquefaction resistance due to the presences of fines (e.g., Chang et al. 1982; Kuerbis et al. 1988; and Yasuda et al. 1994), 3) decrease in liquefaction resistance by the introduction of fines (Troncoso and Verdugo 1985; Sladen et al. 1985; Vaid 1994), 4) a reduction in liquefaction resistance until a certain threshold fines content then an increase in liquefaction strength with increasing fines content (Koester 1994; Lade and Yamamuro 1997; Yamamuro et al. 1999), and 5) liquefaction resistance being more closely related to the sand skeleton void ratio than to its silt content (Troncoso and Verdugo 1985; Troncoso 1990; Kuerbis et al. 1988). The plasticity of the fines content also has important effects on the liquefaction potential. As the plasticity of the fines increase, the soil behavior starts to exhibit cohesive properties. Boulanger and Idriss (2005) suggest that soils with plasticity indices higher than seven should not be included in databases of liquefaction instability.

Fines content and the distribution of fines throughout a soil deposit can affect the timing of failure in relation to the earthquake loading. The pore pressure build-up during the earthquake may not trigger movement if given time the pore pressure will begin to migrate or redistribute based on differences in permeability. If an impermeable layer exists, the migration of pore pressure can concentrate along that layer and induce a flow failure (Kokusho and Kojima 2002). Pore pressure redistribution can cause a delay in failure as what potentially happened during the 1971 Lower San Fernando Dam failure, which was reported to have occurred after earthquake shaking ceased (Castro et al., 1985; and Kulasingam et al., 2004).

In the evaluation of liquefaction potential using SPT test data, the usual approach is to account for the effects of fines content on liquefaction potential by correcting the SPT blow count. There are several corrections available to correct SPT blow counts for fines content in liquefaction potential evaluation, and it is the objective of this research to investigate the applicability of these correction procedures. Procedures to correct for the effects of fines content include those proposed by Seed and Harder (1990), Stark and Mesri (1992), and Youd et al. (2001). The Seed and Harder (1990), and Stark and Mesri (1992) corrections are based on data from cases of flow failure, whereas the Youd et al. (2001) fines content correction is based on data from level ground cases of liquefaction. The Seed and Harder (1990), and Stark and Mesri (1992) corrections use the same form of equation to compute the fines corrected SPT blow count shown below in Eq. (3-10):

$$(N_1)_{60cs} = (N_1)_{60} + \Delta(N_1)_{60} \tag{3-10}$$

where $(N_1)_{60cs}$ is the clean-sand equivalent SPT blow count, $(N_1)_{60}$ is the SPT blow count normalized to 60% energy and one atmospheric pressure, and $\Delta(N_1)_{60}$ is the blow count correction as a function of the fines content. Seed and Harder (1990) suggest the following four

corrections: for FC = 10%, $\Delta(N_1)_{60}$=1; for FC=25%, $\Delta(N_1)_{60}$=2; for FC=50%, $\Delta(N_1)_{60}$=4; and for $FC \geq$75%, $\Delta(N_1)_{60}$=5. Stark and Mesri (1992) suggest the following six corrections: for FC=10%, $\Delta(N_1)_{60}$=2.5; for FC=15%, $\Delta(N_1)_{60}$=4; for FC =20%, $\Delta(N_1)_{60}$=5; for FC=25% $\Delta(N_1)_{60}$=6; for FC =30%, $\Delta(N_1)_{60}$=6.5; and for $FC \geq$35%, $\Delta(N_1)_{60}$=7. For intermediate values of fines content, linear interpolation should be used to determine the correction term. The equation presented by Youd et al. (2001 for adjusting the SPT blow count for fines content correction is given as:

$$(N_1)_{60cs} = \alpha + \beta(N_1)_{60} \tag{3-11}$$

where the terms α and β are defined by the following equations:

$$\alpha = 0 \text{ and } \beta = 1 \text{ for } FC \leq 5\% \tag{3-12}$$

$$\alpha = \exp\left(1.76 - 190/FC^2\right) \text{ and } \beta = 0.99 + FC^{1.5}/1000 \text{ for } 5\% < FC < 35\% \tag{3-13}$$

$$\alpha = 5 \text{ and } \beta = 1.2 \text{ for } FC \geq 35\% \tag{3-14}$$

The SPT data from the flow failure case histories are corrected for fines content using the three procedures described above resulting in the corrected SPT blow counts presented in Table 3-4. Regression analyses using a second-order polynomial are performed on the corrected SPT blow counts and the back-calculated liquefied shear strengths. Figures 3-4, 3-5, and 3-6 contain data and regression lines for the Seed and Harder (1990), Stark and Mesri (1992), and Youd et al. (2001) fines content corrections, respectively. Comparison of the R^2 values for relationships with and without fines content corrections indicate that the relationship without a fines content correction yields the best-fit. Therefore, it is suggested that no fines content correction should be applied to the SPT data for estimating the liquefied shear strength.

Normalization

Although there are several potential advantages of using normalized residual shear strength, as was argued by Stark and Mesri (1992), and Olson and Stark (2002), there are conflicting evidence on the validity of normalizing the residual shear strength with respect to the initial effective vertical stress. The main argument against the use of normalized residual shear strength is the relatively small influence of the overburden stress on the void ratio of sands and gravel particularly for shallow depths. Unlike clays whose void ratio is determined almost uniquely by stress history, cohesionless soils can exhibit a wide range of void ratios for a given stress level. Critical state soil mechanics (Schofield and Wroth, 1968) and the steady-state concept proposed by Poulos et al. (1985) provide another argument against the use of normalized shear stress. Both critical state and steady-state concepts suggest that the residual shear strength (termed the critical or steady shear strength) of soils at large strains is a function only of the grain shape, grain-size distribution, and void ratio but not of the stress history. Thus, for a given void ratio, the critical/steady state is the same regardless of the magnitude of the consolidation stress. The critical/steady state shear strength can be normalized by the initial effective vertical stress if the critical/steady state line is parallel to the consolidation line in the void ratio vs. the logarithm of effective confining stress. There are, however, conflicting experimental evidence on whether the critical/steady state and consolidation lines are indeed parallel for cohesionless soils (Castro, 1997).

Several arguments have also been put forward to support the validity of normalizing the residual shear strength of liquefied soils. Baziar and Dobry (1995) reported residual shear strength correlation based solely on the initial effective vertical stress. Their results, which included both field cases of flow liquefaction and lateral spreading, indicated normalized

residual undrained shear strength between 0.04 and 0.2. Ishihara (1993) has proposed that the quasi-steady-state strength be used in analyses of post-liquefaction stability instead of the critical/steady shear strength. The quasi-state-state occurs at the point where the soil changes from a contractive to a dilative response, and where the shear stress is minimum for contractive-dilative soils (Ishihara, 1993). For very loose sand, the quasi-steady-state and the state-state coincide. Ishihara's suggestion is motivated by the fact that most of the laboratory data on the residual shear strength of cohesionless soils reported in the literature actually correspond to the quasi-steady-state shear strength. Unlike the critical/steady state, the quasi-steady-state is related to the consolidation stress and may be normalized by the initial confining stress (Gutierrez, 2003).

An indication of the validity of using normalized liquefied shear strength can be obtained from the database presented above. Figure 3-7 shows the data in Table 3-4 in terms of the uncorrected SPT blow count vs. normalized liquefied shear strength $S_{u\text{-}LIQ}/\sigma'_v$. The plus and minus one standard deviation lines as presented by Olson and Stark (2003) are also plotted on Figure 3-7, it can be seen that the relationship presented here produces higher estimates of the liquefied shear strength ratio as compared to Olson and Stark (2003). In comparison with Figure 3-3, the data on normalized liquefied shear strength exhibit a wider scatter with an R^2 of only 0.22, indicating that $S_{u\text{-}LIQ}$ correlates better with $(N_1)_{60}$ than $S_{u\text{-}LIQ}/\sigma'_v$. Note that the data shown in Figure 3-7 do not account for kinetics. Olson and Stark (2003) showed better correlation between the normalized liquefied shear strength which account for kinetics and $(N_1)_{60}$.

Conclusions and Recommendations

The following are the main conclusions obtained from the re-analysis and extension of the database on field case histories of flow liquefaction of natural and engineered slopes:

1. Cases analyzed with an infinite slope model and the Spencer's generalized method of slices can be combined to develop a liquefied shear strength relation based on the similarity between the best-fit curves for each type of slope stability analysis.
2. A second-order polynomial provides the highest R^2 value for the liquefied shear strength versus minimum $(N_1)_{60}$ relationship as compared to linear, exponential, logarithmic and power fits.
3. The minimum $(N_1)_{60}$ blow count is used to develop $S_{u\text{-}LIQ}$ relations because flow failures are likely to develop along the "weakest-link". The R^2 value for the liquefied shear strength versus SPT blow count corrected according to Seed and Harder (1990) for fines content is higher than the Stark and Mesri (1992), and Youd et al. (2001) corrections.
4. The R^2 values for relationships developed for fines content corrected SPT blow counts are lower than R^2 values computed for relationships where the SPT blow counts are not corrected for fines content. The author's recommend use of the liquefied shear strength relationship shown in Figure 3-3 without an SPT correction for fines content to estimate $S_{u\text{-}LIQ}$ from the minimum SPT blow count.
5. The liquefied shear strength should not be normalized by the initial vertical effective stress. It appears that insufficient information is available to provide a clear relationship between the minimum SPT blow count, the liquefied shear strength, and the initial vertical effective stress.

Chapter 3 References

Bardet, J.P. and Davis, C.A. (1996). "Performance of San Fernando Dams during 1994 Northridge Earthquake." *J. Geotech. Eng*., *ASCE*, 122(7), 554-564.

Baziar, M.H. and Dobry, R. (1995). "Residual strength and large-deformation potential of loose silty sands." *J. Geotechnical Eng., ASCE*, vol. 121, no. 12, pp. 896-906.

Boulanger, R.W. and Idriss, I.M. (2005). "Evaluating cyclic failure in silts and clays." *Proceedings, Geotechnical Earthquake Engineering: Concepts and Research*. Prepared by TC4 Committee of ICSMGE, Japanese Geotechnical Society, Tokyo, 78-86.

Casagrande, A. (1965). "Second Terzaghi Lecture: The role of "calculated risk" in earthwork and foundation engineering." *J. Soil Mech. Found. Div., ASCE*, 91(SM4), 1-40.

Castro, G. (1975). "Liquefaction and cyclic mobility of saturated sands." *J. Geotech. Eng. Div*., *ASCE*, 116(5), 805-821.

Castro, G. (1995). "Empirical methods in liquefaction evaluation." *Proc., First Annual Leonardo Zeevaert International Conference*, Vol. 1, 1-41.

Castro, G., Poulos, S.J., and Leathers, F.D. (1985). "Re-examination of slide of Lower San Fernando Dam." *J. Geotech. Eng. Div*., *ASCE*, 111(9), 1093-1106.

Castro, G., Keller, T.O., and Boynton, S.S. (1989). "Re-evaluation of the Lower San Fernando Dam: Report 1, an investigation of the February 9, 1971 slide." *U.S. Army Corps of Engineers Contract Report GL-89-2*, Vols. 1 and 2, U.S. Army Corps of Engineers Waterways Experiment Station, Vicksburg, Mississippi.

Castro, G. (1997), "Post-liquefaction shear strength from case-histories," *Proc. NSF Workshop Post-liquefaction Shear Strength of Granular Soils*, http://www.conted.uiuc.edu/Cl/soil/

Cetin, K., Isik, N., and Unutmaz, B. (2004). “Seismically induced landslide at Degirmendere Nose, Izmit Bay during Kocaeli (Izmit)-Turkey earthquake.” *Soil Dyn. Earthq. Eng.*, 24, 189-197.

Cetin, K.O., Youd, T.L., Seed, R.B., Bray, J.B., Sancio, R.B., Lettis, W., Yilmaz, M.T. and Durgunoglu, H.T. (2002). "Liquefaction-induced ground deformations at Hotel Sapanca during Kocaeli (Izmit), Turkey earthquake." *Soil Dyn. Earthq. Eng*: 1083-1092.

Chang, N. Y., Yey, S.T., and Kaufman, L. P. (1982), "Liquefaction potential of clean and silty-sands," *Proc. 3rd Intl. Earthq. Microzonation Conf.,* vol. 2, pp. 1018-1032.

Davis, Jr., A.P., Poulos, S.J. and Castro, G. (1988). “Strengths backfigured from liquefaction case histories.” *2nd Intl. Conf. Case Histories Geotech. Eng*., June 1-5, 1988, St. Louis, Mo. Paper No. 4.35, 1693-1701.

de Alba, P., Seed, H.B., Retamal, E., and Seed, R.B. (1987). “Residual strength of sand from dam failures in the Chilean earthquake of March 3, 1985.” *Earthquake Engineering Research Center Report No. UCB/EERC-87-11*, University of California, Berkeley, CA.

de Alba, P.A., Seed, H.B., Retamal, E., and Seed, R.B. (1988). “Analyses of dam failures in 1985 Chilean earthquake.” *Journal of Geotechnical Engineering, ASCE*, 114(12), 1414-1434.

Dobry, R. and Alvarez, L. (1967). “Seismic failures of Chilean tailings dams.” *J. Soil Mech. Found. Div., ASCE,* 93(SM6), 237-260.

Duncan, J.M. and Wright, S.G. (2005). *Soil Strength and Slope Stability*. McGraw-Hill, New Jersey.

Fear, C.E., and McRoberts, E.C. (1995). "Reconsideration of initiation of liquefaction in sandy soils. *J. Geotech. Engr. ASCE*. 121(3), 249-261.

Gutierrez, M. (2003), "Modeling of the Steady-State Response of Granular Soils," *Soils and Foundations*, vol. 43, no.5, pp. 93-105

Gutierrez, M., Duncan, J.M., Woods, C. and Eddy, M. (2003). "Development of a simplified reliability-based method for liquefaction evaluation." *Report for USGS Grant Number 02HQGR0058*

Hazen, A. (1918). "A study of the slip in the Calaveras Dam." *Engineering News-Record*, 81(26), 1158-1164.

Hazen, A. (1920). "Hydraulic-fill dams." *Transactions of the American Society of Civil Engineers*, Paper No. 1458, 1713-1821 (including discussions).

Hazen, A. and Metcalf, L. (1918). "Middle section of upstream side of Calaveras dam slips into reservoir." *Engineering News-Record*, 80(14), 679-681.

Hryciw, R.D., Vitton, S., and Thomann, T.G. (1990). "Liquefaction and flow failure during seismic exploration." *Journal of Geotechnical Engineering*, ASCE, 116(12), 1881-1899.

Ishihara, K. (1984). "Post-earthquake failure of a tailings dam due to liquefaction of the pond deposit." *Proc., Inter. Conf. on Case Histories in Geotechnical Engineering*, Rolla, Missouri, May 6-11, Vol. 3, 1129-1143.

Ishihara, K. (1993). "Liquefaction and flow failure during earthquakes." 33rd Rankine Lecture. *Geotechnique*, 43(3), 351-415.

Ishihara, K., Yasuda, S. and Yoshida, Y. (1990). "Liquefaction-induced flow failure of embankments and residual strength of silty sands." *Soils Founds.*, 30(3), 69-80.

Ishihara, K., Okusa, S., Oyagi, N. and Ischuk, A. (1990). "Liquefaction-induced flow slide in the collapsible loess deposit in Soviet Tajik." *Soils Founds*, 30(4), 73-89.

Jitno, H. and Byrne, P.M. (1995). “Predicted and observed liquefaction response of Mochikoshi tailings dam.” *Proc., 1st International Conf. on Earthquake Geotechnical Engineering*, Nov. 14-16, Tokyo, Japan, Vol. 2, 1085-1090.

Koester, J. P. (1994), "The influence of fines type and content on cyclic strength," in *Ground Failures under Seismic Conditions, Geotech. Spl. Publ.* No. 44, S. Prakash, and P. Dakoulas, (eds.), ASCE, pp. 17-33.

Kokusho, T. and Kojima, T. (2002). " Mechanism for Postliquefaction Water Film Generation in Layered Sand."*J. Geotech. Geoenvir. Eng.*, *ASCE*, 128(2), 129-137.

Konrad, J.M. and Watts, B.D. (1995). “Undrained shear strength for liquefaction flow failure analysis.” *Can. Geotech. J.,* 32, 783-794.

Kuerbis, R., Negussey, D. and Vaid, Y. P. (1988), "Effect of gradation and fines content on the undrained response of sand," in *Hydraulic Fill Structures, Geotech. Specl. Publ.* No. 21, D.J.A. Van Zyl and S.G. Vick (eds.), ASCE, pp. 330-345.

Kulasingam, R., Malvick, E.J., Boulanger, R.W., and Kutter, B.L. "Strength loss and localization at silt interlayers in slopes of liquefied sand." *J. Geotech. Engr. ASCE*. 130(11), 1192-1202.

Lade, P. V. and Yamamuro, J. A. (1997), "Effects of nonplastic fines on static liquefaction of sands," *Can. Geotech. J.,* vol. 34, pp. 918-928.

Lee, K.L., Seed, H.B., Idriss, I.M., and Makdisi, F.I. (1975). “Properties of soil in the San Fernando hydraulic fill dams.” *Journal of the Geotechnical Engineering Division*, *ASCE*, 101(GT8), 801-821.

Lucia, P.C. (1981). “Review of experiences with flow failures of tailings dams and waste impoundments.” Ph.D. Thesis, University of California, Berkeley, Calif.

Marcuson, W.F., III, Ballard, R.F., Jr. and Cooper, S.S. (1978). "Comparison of penetration resistance values to in situ shear wave velocities." *Proc. 2nd Intl. Conf. Microzonation for Safer Construction – Research and Application*, San Francisco, CA, Nov. 26–Dec. 1, 2, 1013-1023.

Marcuson, W.F., III, Ballard, R.F., Jr, and Ledbetter, R.H. (1979). "Liquefaction failure of tailings dams resulting from the Near Izu Oshima earthquake, 14 and 15 January, 1978." *Proc. 6th Pan-Am. Conf. Soil Mech. Fnd. Eng.*, Lima Peru, 2, 69-80.

Marcuson, W.F., III, Hynes, M.E., and Franklin, A.G. (1990). "Evaluation and use of residual strength in seismic safety analysis of embankments." *Earthquake Spectra*, 6(3), 529-572.

Matsuo, O., Saito,Y., Sasaki, T., Kondoh, K. and Sato, T. (2002). "Earthquake-induced flow slides of fills and infinite slopes." *Soils Founds.*, 42, 1, 89-104.

Middlebrooks, T.A. (1942). "Fort Peck slide." *Trans. Am. Soc. Civil Engr.*, 107, 723-764.

Mishima, S. and Kimura, H. (1970). "Characteristics of landslides and embankment failures during the Tokachioki earthquake." *Soils Founds.*, 10(2), 39-51.

Mittal, H.K. and Hardy, R.M. (1977). "Geotechnical aspects of a tar sand tailings dyke." *Proc. Conf. Geotech. Practice for Disposal of Solid Waste Materials*, *ASCE Specialty Conf. Geotech. Eng.* Div., 1, 327-347.

Miura, K., Yoshida, N., and Wakamatsu, K. (1995). "Damage to fill embankment during the 1993 Kushiro-oki earthquake." *Proc., 1st International Conf. on Earthquake Geotechnical Engineering*, Nov. 14-16, Tokyo, Japan, Vol. 2, 1057-1062.

Miura, K., Yoshida, N., Nishimura, M., and Wakamatsu, K. (1998). "Stability analysis of the fill embankment damaged by recent two major earthquakes in Hokkaido, Japan." *Proc., 1998 Geotechnical Earthquake Engineering and Soil Dynamics Specialty Conference, ASCE*

Geo-Institute Geotechnical Special Publication No. 75, Vol. 2, August 3-6, Seattle, Washington, 926-937.

Ohya, S., Iwasaki, T., and Wakamatsu, M. (1985). "Comparative study of various penetration tests in ground that underwent liquefaction during the 1983 Nihon-Kai-Chubu and 1964 Niigata earthquakes." *Proc., Workshop on In situ Testing Methods for Evaluation of Soil Liquefaction Susceptibility*, San Francisco, California, Vol. 1, 56-88.

Okusa, S. and Anma, S. (1980). "Slope failures and tailings dam damage in the 1978 Izu-Ohshima-Kinkai earthquake." *Engineering Geology*, 16, 195-224.

Okusa, S., Anma, S., and Maikuma, H. (1980). "Liquefaction of mine tailings in the 1978 Izu-Ohshima-Kinkai earthquake, central Japan." *Proc., 7th World Conf. on Earthquake Engineering*, Sept. 8-13, Istanbul, Turkey, Vol. 3, 89-96.

Okusa, S., Anma, S., and Maikuma, M. (1984). "The propagation of liquefaction pressure and delayed failure of a tailings dam dike in the 1978 Izu-Oshima-Kinkai earthquake." *Proc. 8th World Conf. Earthq. Eng.*, July 21-28, San Francisco, CA, 1, 389-396.

Olson, S.M. (2001). "Liquefaction analysis of level and sloping ground using field case histories and penetration resistance." *Ph.D. Thesis*, University of Illinois, Urbana-Champaign, Illinois.

Olson, S.M. and Stark, T.D. (2003). "Liquefied strength ratio from liquefaction flow failure case histories." *Can. Geotech. J.*, 39, 629-647.

Olson, S.M., Stark, T.D., Walton, W.H., and Castro, G. (2000). "Static liquefaction flow failure of the North Dike of Wachusett Dam." *J. Geotech. Geoenvir. Eng., ASCE*, 126(12), 1184-1193.

Olson, S.M. and Stark, T.D. (2002), "Liquefied shear strength ratio from liquefaction flow failure case histories," *Canadian Geotech. J*., vol. 39, no. 3, pp. 629-647.

Ozutsumi, O., Sawada, S., Takeshima, Y., Sugiyami, W., and Shimazu, T. (2002). "Effective stress analyses of liquefaction-induced deformation in river dikes." *Soil Dynamics and Earthquake Engineering*, vol. 22: 1075-1082.

PEER (2000). "Documenting incidents of ground failure resulting from the August 17, 1999 Kocaeli, Turkey Earthquake." PEER, Berkeley, CA, http://peer.berkeley.edu/turkey/adapazari/.

Plewes, H.D., O'Neil, G.D., McRoberts, E.C. and Chan, W.K. (1989). "Liquefaction considerations for Suncor tailings pond." *Proc. Dam Safety Seminar*, Edmonton, Alberta, 1, 61-89.

Poulos, S.J., Castro, G. and France, W. (1985). "Liquefaction evaluation procedure." *J. Geotechnical Eng., ASCE*, vol. 111, no. 6, pp. 772-792.

PWRI (1971). "Survey on disaster caused by the Tokachi-oki Earthquake 1968." *Report Public Works Research Institute*, 141, 67-77 (in Japanese).

Rathje, E.M., Karatas, I., Wright, S.G. and Bachhuber, J. (2004). "Coastal failures during the 1999 Kocaeli Earthquake in Turkey." *Soil Dyn. Earthq. Eng*., 24, 699-712.

Ross, G.A. (1968). "Case studies of soil stability problems resulting from earthquakes." Ph.D. Thesis, University of California, Berkeley, Calif.

Schofield, A.N. and Wroth, C.P. (1968). *Critical State Soil Mechanics.* London: McGraw-Hill.

Seed, H.B. (1987). "Design problems in soil liquefaction." *J. Geotech. Eng.*, *ASCE*, 113(8), 827-845.

Seed, H.B. and Harder, L.F. (1990). "SPT-based analysis of cyclic pore pressure generation and undrained residual strength." *Proc. H.B. Seed Mem. Symp*., 2, 351-376.

Seed, H.B., Lee, K.L., Idriss, I.M., and Makdisi, F. (1973). "Analysis of the slides in the San Fernando Dams during the earthquake of Feb. 9, 1971." *Earthquake Engineering Research Center 73-2*, University of California, Berkeley, Calif.

Seed, H.B., Lee, K.L., Idriss, I.M., and Makdisi, F. (1975). "Dynamic analysis of the slide in the Lower San Fernando Dam during the earthquake of February 9, 1971." *Journal of the Geotechnical Engineering Division*, ASCE, 101(GT9), 889-911.

Sladen, J. A., D'Hollander, R. D. and Krahn, J. (1985), "Back analysis of the Nerlerk berm liquefaction slides, *Can. Geotech. J.* vol. 2, pp. 579-588.

Spiegel, M.R. and Stephens, L.J. (1999). *Statistics*. 3rd Edition., McGraw-Hill, New Jersey

Spencer, E. (1967). "A method of analysis of the stability of embankments assuming parallel interslice forces." *Géotechnique*, London, 17(1), 11-26.

Sully, J.P., Fernandez, A., and Zalzman, S. (1995). "Back-analysis of deformations for case histories involving flow-type failures." *Proc., 3rd International Conf. on Recent Advances in Geotechnical Earthquake Engineering and Soil Dynamics*, April 2-7, St. Louis, MO, Vol. 1, 499-502.

Stark, T.D. and Mesri, G.M. (1992). "Undrained shear strength of liquefied sands for stability analysis." *J. Geotecch. Eng., ASCE*, 118(11), 1727-1747.

Tocher, D. (1959). "Seismographic results from the 1957 San Francisco earthquakes." *In Special Report 57*, State of California Division of Mines, San Francisco, CA.

Towhata, I., Ghalandarzadeh, A., Sundarraj, K.P. and Vargas-Monge, W. (1996). "Dynamic failures of subsoils observed in waterfront areas." *Soils Founds.*, January 1996 *Special Issue*, 149-160.

Troncoso, J. H. (1990), "Failure risks of abandoned tailings dams," *Proc. Intl. Symp. Safety Rehabilitation of Tailing Dams,* International Commission on Large Dams, Paris, pp. 82-89.

Troncoso, J. H. and Verdugo, R. (1985), "Silt content and dynamic behavior of tailing sands," *Proc. 11th Intl. Conf. Soil Mech. Fnd. Eng.,* vol. 3, pp. 1311-1314.

Vaid, Y.P. (1994), "Liquefaction of silty soils," in *Ground Failures under Seismic Conditions, Geotech. Spl. Publ.* No. 44, S. Prakash and P. Dakou1as (eds.), ASCE, pp. 1-16.

Vasquez-Herrera, A. and Dobry, R. (1989). "Re-evaluation of the Lower San Fernando Dam: Report 3, the behavior of undrained contractive sand and its effect on seismic liquefaction flow failures of earth structures." *U.S. Army Corps of Engineers Contract Report GL-89-2*, U.S. Army Corps of Engineers Waterways Experiment Station, Vicksburg, Mississippi.

U.S. Army Corps of Engineers. (1939). "Report on the slide of a portion of the upstream face of the Fort Peck Dam, Fort Peck, Montana." *U.S. Govt. Printing Office*, Washington, D.C.

Yamada, G. (1966). "Damage to earth structures and foundations by the Niigata earthquake June 16, 1964, in JNR." *Soils Founds.,* 6(1), 1-13.

Yamamuro, J. A., Covert, K. M. and Lade, P. V. (1999), "Static and cyclic liquefaction of silty sands," *Proc. Intl. Workshop Physics and Mechanics of Soil Liquefaction,* P. V. Lade, and J.A. Yamamuro (eds.), pp. 55-65

Yasuda, S., Wakamatsu, K. and Nagase, H. (1994), "Liquefaction of artificially filled silty sands," in *Ground Failures under Seismic Conditions, Geotech. Spl. Publ.* No. 44, S. Prakash and P. Dakoulas, (eds.), ASCE, pp. 91-104.

Yegian, M.K., Ghahraman, V.G., and Harutinunyan, R.N. (1994). "Liquefaction and embankment failure case histories, 1988 Armenia earthquake." *J. Geotech. Eng.,, ASCE*, 120(3), 581-596.

Youd, T.L. and Bennett, M.J. (1983). "Liquefaction sites, Imperial Valley, California." *J. Geotech. Eng.*, *ASCE*, 109(3), 440-457.

Youd, T.L., Idriss, I.M., Andrus, R.D., Arango, I., Castro, G., Christian, J.T., Dobry, R.,Finn, L.D.L, Harder, L.F.Jr., Hynes, M.E., Ishihara, K., Koester, J.P., Liao, S.S.C., Marcuson, W.F.III, Martin, G.R., Mitchell, J.K., Moriwaki, Y., Power, M.S., Robertson, P.K., Seed, R.B. and Stokoe, K.H.II. (2001). "Liquefaction resistance of soils: Summary report from the 1996 NCEER and 1998 NCEER/NSF workshops on evaluation of liquefaction resistance of soils." *J. Geotech. Geoenvir. Eng., ASCE*, 127(10), 817-833.

Chapter 3 Tables:

Table 3-1 - Case histories of flow liquefaction back-analyzed to develop liquefied shear strength relationships.

ID #	Case History	References	Cause of Failure
1	Calaveras Dam	Olson (2001), Hazen and Metcalf (1918), Hazen (1918), Hazen (1920)	1918 Construction
2	Cark Canal	PEER (2000)	1999 Kocaeli EQ
3	Chonan Middle School	Olson (2001), Ishihara et al. (1990a), Ishihara (1993)	1987 Chibi-Taho-oki EQ
4	Cumhuriyet	PEER (2000)	1999 Kocaeli EQ
5	Degirmendere Nose	PEER (2000), Cetin et al. (2004)	1999 Kocaeli EQ
6	El Cobre Tailings Dam	Dobry and Alvarez (1967), Olson (2001), Olson and Stark (2003)	1965 Chile EQ
7	Esme Nose	Rathje et al. (2004)	1999 Kocaeli EQ
8	Fort Peck Dam	US Army Corps of Engineers (1939), Middlebrooks (1942), Casagrande (1965), Marcuson et al. (1978), Seed (1987), Davis et al. (1988), Seed and Harder (1990), Stark and Mesri (1992), Wride et al. (1999), Olson (2001), Olson and Stark (2003)	1934 Construction
9	Hachiro-Gato Roadway Embankment	Olson (2001), Ohya et al. (1985)	1983 Nihon-kai-Chubu EQ
10	Heber Road	Youd and Bennett (1983), Davis et al. (1988), Stark and Mesri (1992), Wride et al. (1999)	1979 Imperial Valley EQ
11	Hokkaido Tailings Dam	Ishihara et al. (1990a), Olson (2001), Olson and Stark (2003)	1968 Tokachi-oki EQ
12	Hotel Sapanca	PEER (2000), Cetin et al. (2002)	1999 Kocaeli EQ
13	Itoizawa Road Fill	PWRI (1971), Matsuo et al. (2002)	1993 Kushiro-oki EQ
14	Koda Numa Highway Embankment	Mishima and Kimura (1970), Lucia (1981), Seed (1987), Seed and Harder (1990), Stark and Mesri (1992), Wride et al. (1999), Olson (2001), Olson and Stark (2003)	1968 Tokachi-oki EQ
15	La Marquesa Dam (Downstream)	Sully et al. (1995), Castro (1995), de Alba et al. (1987, 1988), Olson (2001)	1985 Chile EQ
16	La Marquesa Dam (Upstream)	Same as La Marquesa Dam (Downstream)	1985 Chile EQ
17	La Palma Dam	Jitno and Byrne (1995), de Alba et al. (1987, 1988), Castro (1995), Olson (2001)	1985 Chile EQ
18	Lake Ackerman Roadway Embankment	Olson (2001), Hryciw et al. (1990), Sully et al. (1995)	1987 Seismic Survey
19	Lake Merced Bank	Tocher (1958), Ross (1968)	1957 San Francisco EQ
20	Lower San Fernando Dam	Castro et al. (1989), Davis et al. (1988), Marcuson et al. (1990), Seed (1987), Seed et al. (1973), Seed et al. (1975), Lee et a. (1975), Seed and Harder (1990), Vasquez-Herrera and Dobry (1989), Stark and Mesri (1992), Wride et al. (1999), Olson (2001)	1971 San Fernando EQ
21	May 1 Slide	Ishihara et al. (1990b), Olson (2001), Olson and Stark (2003)	1989 Tajik EQ
22	Metoki Road Embankment	PWRI (1971), Ishihara et al. (1990a), Matsuo et al. (2002), Olson (2001)	1968 Tokachi-oki EQ
23	Mochikoshi Dike 1	Marcuson et al. (1979), Okusa and Anma (1980), Okusa et al. (1980, 1984), Ishihara (1984), Davis et al. (1988), Ishihara et al. (1990a), Olson (2001)	1978 Izu-Ohshima-Kinkai EQ
24	Mochikoshi Dike 2	Same as Mochikoshi Dike 1	1979 Izu-Ohshima-Kinkai EQ
25	Nalband Railway Embankment	Yegian et al. (1994), Olson (2001)	1988 Armenia EQ
26	Niteko Middle Dam	Towhata et al. (1996)	1995 Hyogoken-Nambu EQ
27	Niteko Upper Dam	Towhata et al. (1996)	1995 Hyogoken-Nambu EQ
28	River Park	Youd and Bennett (1983)	1979 Imperial Valley EQ
29	Route 272	Olson (2001), Olson and Stark (2003)	1993 Kushiro-oki EQ
30	Seyman Tea Garden	PEER (2000)	1999 Kocaeli EQ
31	Shibecha-Cho Embankment	Miura et al. (1995, 1998), Olson (2001)	1993 Kushiro-oki EQ
32	Shiribeshi-Toshibetsu Site 3	Ozutsumi et al. (2002)	1993 Hokkaido-Nansei-oki EQ
33	Shiribeshi-Toshibetsu Site 5	Ozutsumi et al. (2002)	1993 Hokkaido-Nansei-oki EQ
34	Tar Island Dyke	Mittal and Hardy (1977), Plewes et al. (1989), Konrad and Watts (1995), Olson (2001), Olson and Stark (2003)	1972-1974 Construction
35	Uetsu-Line Railway Embankment	Yamada (1966), Lucia (1981), Seed (1987), Seed and Harder (1990), Wride et al. (1999), Olson (2001), Olson and Stark (2003)	1964 Niigata EQ
36	Upper San Fernando Dam	Seed et al. (1975), Lee et al. (1975), Seed (1987), Seed and Harder (1990), Bardet and Davis (1996)	1971 San Fernando EQ
37	Wachusett Dam (North Dike)	Olson et al. (2000), Olson (2001)	1907 Initial Filling
38	Yodo Site 6	Ozutsumi et al. (2002)	1995 Hyogoken-Nambu EQ

Table 3-2 - Parameters for the cases of flow failure analyzed with the infinite slope model.

ID #	H_w, m	H_d, m	γ_{sat}, kN/m^3	γ_m, kN/m^3	α, °
2	1.8	2.6	20.5	17.5	1.00
4	3.6	1.1	16.0	15.0	1.72
5	1.7	1.7	22.0	21.0	8.90
6	2.0	0.0	13.4	12.0	4.00
7	7.0	1.0	22.0	21.0	3.00
10	1.5	2.0	20.0	18.0	1.50
11	3.0	0.0	19.6	17.5	4.50
12	6.0	1.2	22.0	21.0	0.80
13	3.5	0.0	20.0	18.0	6.00
22	2.0	0.0	18.1	16.0	4.00
23	4.0	0.0	17.6	15.0	8.00
24	4.0	0.0	17.6	15.0	9.60
26	3.1	0.0	20.0	18.0	4.00
27	2.8	0.0	20.0	18.0	4.80
28	2.0	1.0	20.0	18.0	14.00
29	3.5	1.5	16.5	14.0	4.50
30	12.0	1.0	21.5	20.0	2.00
34	9.0	0.0	18.0	14.5	4.00

Table 3-3 – Types of soils and material properties for the cases of flow failure analyzed with Spencer's generalized method of slices. Total unit weights, γ, have units of kN/m^3 and S_u and c' values have units of kPa.

ID #	Material Parameters		Value
1	Foundation	ϕ'	40.0
		γ	15.7
	Core	ϕ'	32.5
		γ	15.7
	NL Shells	ϕ'	32.5
		γ	17.5
	Liquefied Fill	γ	17.5
3	NL Fill	ϕ'	34.0
		γ	18.1
	Dense Sand	ϕ'	40.0
		γ	20.0
	Liquefied Fill	γ	18.1
8	Foundation	ϕ'	42.0
		γ	20.0
	Core	ϕ'	30.0
		γ	17.5
	NL Shells	ϕ'	30.0
		γ	17.5
	Liquefied Fill	γ	17.5
9	NL Soil	ϕ'	30.0
		γ	18.1
	Liquefied Soil	γ	18.1
14	Foundation	ϕ'	40.0
		γ	20.0
	NL Soil	ϕ'	30.0
		γ	16.0
	Liquefied Soil	γ	16.0
15, 16	Core	S_u	23.9
		γ	16.0
	NL Shells	ϕ'	30.0
		γ	16.0
	Liquefied Fill	γ	16.0
17	Foundation Clay and Sand	ϕ'	37.0
		γ	18.0
	Foundation Sand	ϕ'	32.0
		γ	20.0
	Core	S_u	23.9
		γ	17.0
	NL Shells	ϕ'	32.0
		γ	17.0
	Liquefied Soil	γ	17.0
18	NL Fill	ϕ'	32.0
		γ	19.3
	Dense Sand	ϕ'	40.0
		γ	20.0
	Liquefied Fill	γ	19.3
19	NL Fill	ϕ'	35.0
		γ	19.6
	Foundation	ϕ'	40.0
		γ	19.6
	Liquefied Fill	γ	19.6
20	Alluvium	ϕ'	40.0
		γ	20.0
	NL Fill	ϕ'	32.5
		γ	17.0
	Ground Shale	ϕ'	32.5
		γ	18.0
	Core	S_u	28.3
		γ	17.0
	Liquefied Fill	γ	17.0
21	NL Soil	ϕ'	30.0
		γ	17.0
	Base Soil	ϕ'	30.0
		γ	17.0
	Liquefied Soil	γ	17.0
25	NL Soil	ϕ'	32.5
		γ	17.0
	Volcanic Tuff	ϕ'	40.0
		γ	18.0
	Liquefied Soil	γ	17.0
31	Peat	ϕ'	32.5
		γ	15.0
	NL Soil	ϕ'	32.5
		γ	15.0
	Base Soil	ϕ'	40.0
		γ	20.0
	Liquefied Soil	γ	15.0
32	Asg2	ϕ'	42.0
		γ	16.5
	Upper Ac2	ϕ'	39.0
		γ	16.5
	Ac1	ϕ'	30.0
		γ	16.5
	Embankment	ϕ'	20.0
		c'	25.0
		γ	16.5
	Liquefied Soil	γ	16.5
33	Ac2	ϕ'	39.0
		γ	16.5
	Asa	ϕ'	28
		γ	16.5
	Aca	ϕ'	28
		γ	16.5
	Embankment	ϕ'	20.0
		c'	25.0
		γ	16.5
	Liquefied Soil	γ	16.5
35	NL Soil	ϕ'	32.5
		γ	18.8
	Base Soil	ϕ'	40.0
		γ	20.0
	Liquefied Soil	γ	18.8
36	NL Soil	ϕ'	35.0
		γ	18.0
	Foundation	ϕ'	40.0
		γ	20.0
	Liquefied Soil	γ	18.0
37	NL Soil	ϕ'	32.5
		γ	19.2
	Foundation	ϕ'	40.0
		γ	20.0
	Liquefied Soil	γ	19.2
38	As2-1	ϕ'	28
		γ	16.5
	Upper Ac	ϕ'	34.1
		γ	16.5
	Upper As2-2	ϕ'	28
		γ	16.5
	B3-s	ϕ'	38
		γ	16.5
	Embankment	ϕ'	20.0
		c'	25.0
		γ	16.5
	Liquefied Soil	γ	16.5

Table 3-4 - Minimum SPT blow count data for the case histories listed in Table 3-1 along with the back-calculated liquefied shear strengths and fines content corrected SPT values using three corrections per Seed and Harder (1990), Stark and Mesri (1992), and Youd et al. (2001).

ID #	Available Data	min $(N_1)_{60}$	$S_{u\text{-}LIQ}$	σ'_{vo} (kPa)	$S_{u\text{-}LIQ}/\sigma'_{vo}$	FC (%)	Seed and Harder		Stark and Mesri		Youd et al.		
							$\Delta(N_1)_{60}$	$(N_1)_{60cs}$	$\Delta(N_1)_{60}$	$(N_1)_{60cs}$	α	β	$(N_1)_{60cs}$
1	Est.	5.0	6.5	294.3	0.022	30.0	2.0	7.0	6.5	11.5	4.71	1.15	10.5
2	SPT; CPT	3.0	1.44	60.5	0.024	72.6	4.0	7.0	7.0	10.0	5.00	1.20	8.6
3	SPT	5.2	10.2	56.4	0.181	18.0	1.0	6.2	4.0	9.2	3.23	1.07	8.8
4	SPT; CPT	4.0	2.22	38.8	0.057	84.6	5.0	9.0	7.0	11.0	5.00	1.20	9.8
5	SPT; CPT	8.0	11.17	56.4	0.198	16.7	1.0	9.0	4.0	12.0	2.94	1.06	11.4
6	SPT	1.0	1.87	93.2	0.020	93.0	5.0	6.0	7.0	8.0	5.00	1.20	6.2
7	SPT; CPT	6.0	9.15	106.3	0.086	45.0	2.0	8.0	7.0	13.0	5.00	1.20	12.2
8	SPT; DR	5.0	2.9	319.7	0.009	55.0	4.0	9.0	7.0	12.0	5.00	1.20	11.0
9	SPT; CPT	3.0	1.15	30.2	0.038	15.0	1.0	4.0	4.0	7.0	2.50	1.05	5.6
10	SPT	3.0	1.72	51.3	0.034	17.0	1.0	4.0	4.0	7.0	3.01	1.06	6.2
11	CPT	1.0	4.60	59.9	0.077	50.0	4.0	5.0	7.0	8.0	5.00	1.20	6.2
12	SPT; CPT	2.8	2.20	98.3	0.022	10.0	1.0	3.8	2.5	5.3	0.87	1.02	3.7
13	SPT	5.0	7.27	87.0	0.084	0.0	0.0	5.0	0.0	5.0	0.00	1.00	5.0
14	Est.	2.4	0.5	20.9	0.024	13.0	1.0	3.4	2.5	4.9	1.89	1.04	4.4
15	SPT	5.5	7.30	46.0	0.159	30.0	2.0	7.5	6.5	12.0	4.71	1.15	11.1
16	SPT	4.0	1.55	51.4	0.030	20.0	1.0	5.0	5.0	9.0	3.61	1.08	7.9
17	SPT	3.0	6.20	39.7	0.156	15.0	1.0	4.0	4.0	7.0	2.50	1.05	5.6
18	SPT	3.0	3	40.5	0.074	0.0	0.0	3.0	0.0	3.0	0.00	1.00	3.0
19	SPT	5.0	8	55.4	0.144	2.5	0.0	5.0	0.0	5.0	0.00	1.00	5.0
20	SPT; CPT	6.0	5.20	166.70	0.031	50.0	4.0	10.0	7.0	13.0	5.00	1.20	12.2
21	CPT	5.0	10.50	106.0	0.099	100.0	5.0	10.0	7.0	12.0	5.00	1.20	11.0
22	Est.	3.0	2.52	34.8	0.072	0.0	0.0	3.0	0.0	3.0	0.00	1.00	3.0
23	SPT; CPT	4.0	9.70	73.8	0.131	77.5	5.0	9.0	7.0	11.0	5.00	1.20	9.8
24	SPT; CPT	4.0	11.58	69.2	0.167	77.5	5.0	9.0	7.0	11.0	5.00	1.20	9.8
25	SPT	6.0	6.5	48.9	0.133	17.5	1.0	7.0	4.0	10.0	3.13	1.06	9.5
26	SPT	3.0	4.67	131.8	0.035	15.0	1.0	4.0	4.0	7.0	2.50	1.05	5.6
27	SPT	5.0	4.31	83.7	0.051	15.0	1.0	6.0	4.0	9.0	2.50	1.05	7.7
28	SPT	7.0	13.61	46.2	0.295	0.0	0.0	7.0	0.0	7.0	0.00	1.00	7.0
29	SPT	4.0	6.2	52.3	0.119	21.0	1.0	5.0	5.0	9.0	3.78	1.09	8.1
30	SPT; CPT	6.0	9.70	160.3	0.061	30.0	2.0	8.0	6.5	12.5	4.71	1.15	11.6
31	Est.	5.0	5.2	66.0	0.079	20.0	1.0	6.0	5.0	10.0	3.61	1.08	9.0
32	SPT	2.0	4.50	66.2	0.068	30.0	2.0	4.0	6.5	8.5	4.71	1.15	7.0
33	SPT	2.0	5	49.7	0.101	30.0	2.0	4.0	6.5	8.5	4.71	1.15	7.0
34	SPT; CPT	7.0	11.27	135.8	0.083	17.5	1.0	8.0	4.0	11.0	3.13	1.06	10.6
35	Est.	3.0	1.15	51.7	0.022	1.0	0.0	3.0	0.0	3.0	0.00	1.00	3.0
36	SPT	7.0	15	147.3	0.102	47.5	2.0	9.0	7.0	14.0	5.00	1.20	13.4
37	SPT	4.0	3.6	141.6	0.025	7.5	0.0	4.0	0.0	4.0	0.20	1.01	4.2
38	SPT	3.5	6.50	92.8	0.070	30.0	2.0	5.5	6.5	10.0	4.71	1.15	8.7

Table 3-5 - Results from regression analyses of the flow failure case histories presented in Table 3-1.

Form	Regression Eq.	R^2
Linear	$S_{u\text{-}LIQ} = 1.42(N_1)_{60}$	0.50
Logarithmic	$S_{u\text{-}LIQ} = 4.93\ln((N_1)_{60}) - 0.73$	0.38
Power	$S_{u\text{-}LIQ} = 1.25((N_1)_{60})^{0.96}$	0.32
Exponential	$S_{u\text{-}LIQ} = 1.21\exp(0.31(N_1)_{60})$	0.42
2nd Order Polynomial	$S_{u\text{-}LIQ} = 0.87(N_1)_{60} + 0.1(N_1)_{60}^2$	0.54

Chapter 3 Figures

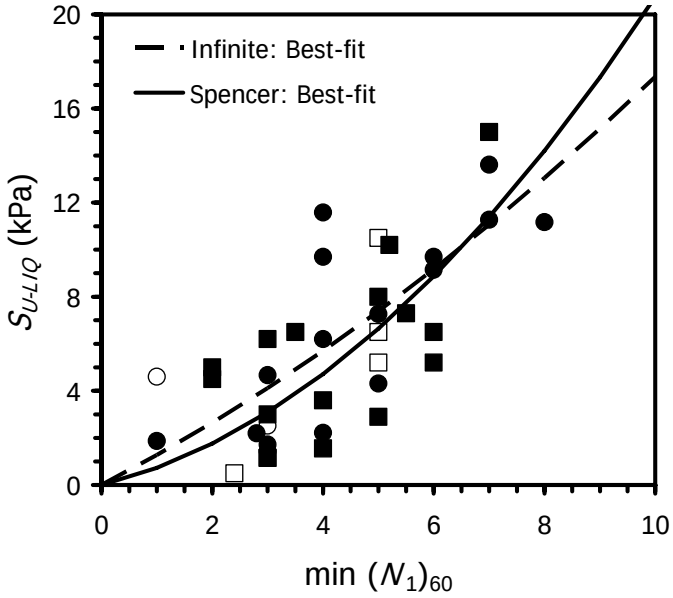

Figure 3-1 - Best-fit second-order polynomial regression lines for flow liquefaction cases analyzed with the infinite slope (R^2 = 0.6) and Spencer generalized method of slices (R^2 = 0.5) slope stability procedures.

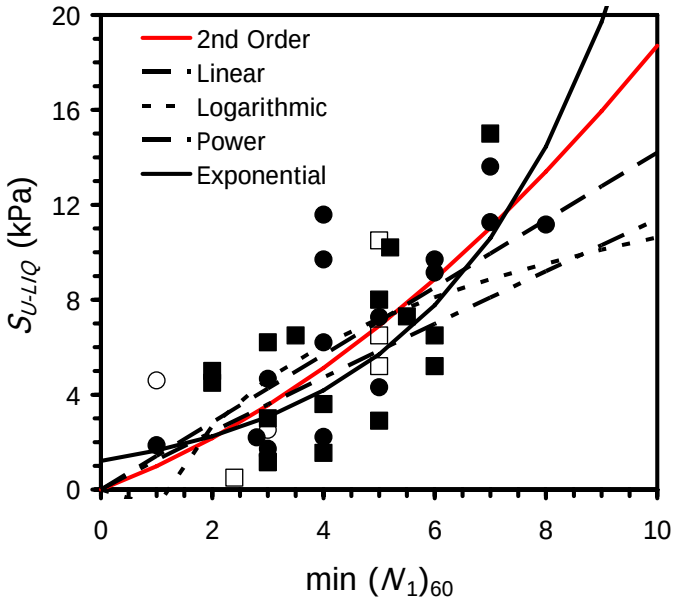

Figure 3-2 - Comparison of different regression equations for liquefied shear strength versus minimum SPT blow count. The equations and R^2 values for each of the regression lines are presented in Table 3-5.

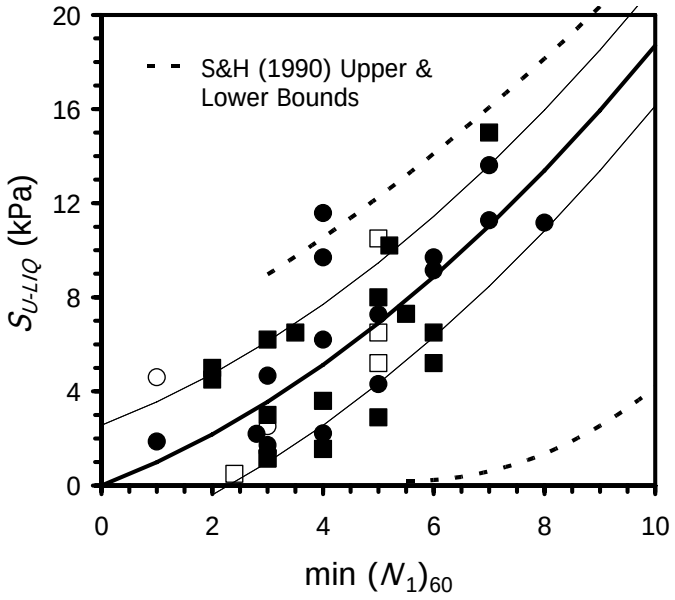

Figure 3-3 - Best-fit second-order polynomial regression for liquefied shear strength versus minimum SPT blow count without fines correction together with plus and minus one standard deviation lines (R^2 = 0.54). The upper and lower bounds as presented by Seed and Harder (1990) are also plotted for comparison.

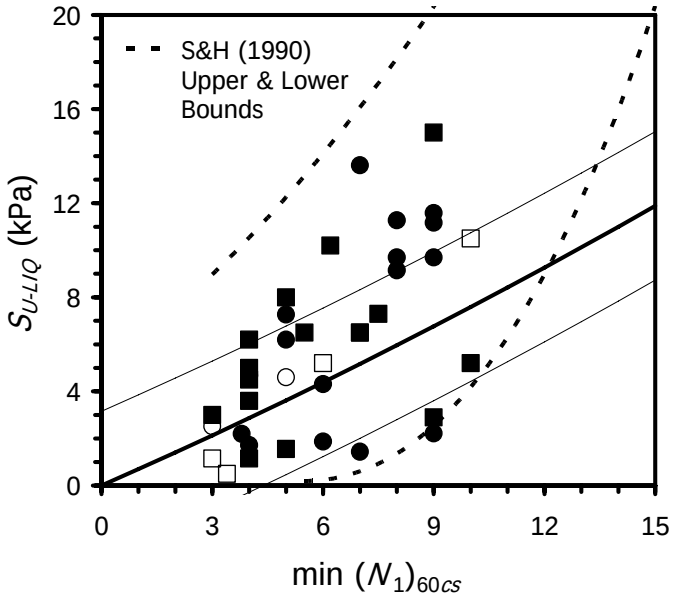

Figure 3-4 - Best-fit second-order polynomial regression for liquefied shear strength versus minimum SPT blow count corrected according to Seed and Harder (1990) together with plus and minus one standard deviation lines ($R^2 = 0.33$).

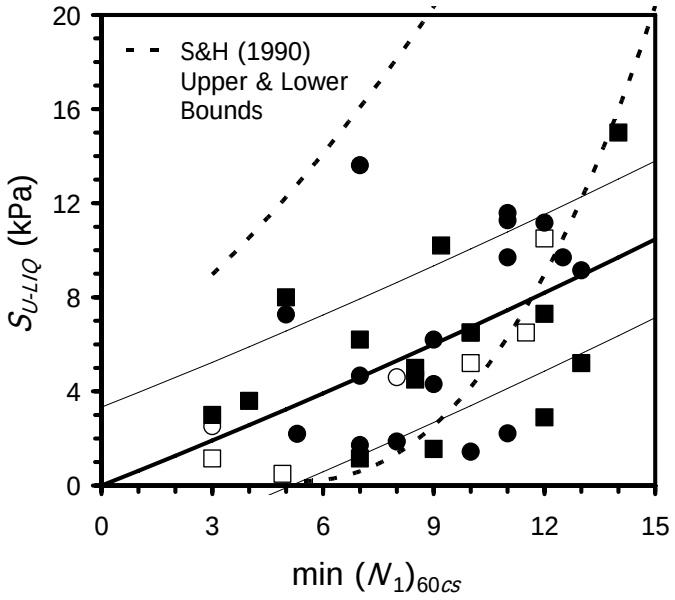

Figure 3-5 - Best-fit second-order polynomial regression for liquefied shear strength versus minimum SPT blow count corrected according to Stark and Mesri (1992) together with plus and minus one standard deviation lines (R^2 = 0.26).

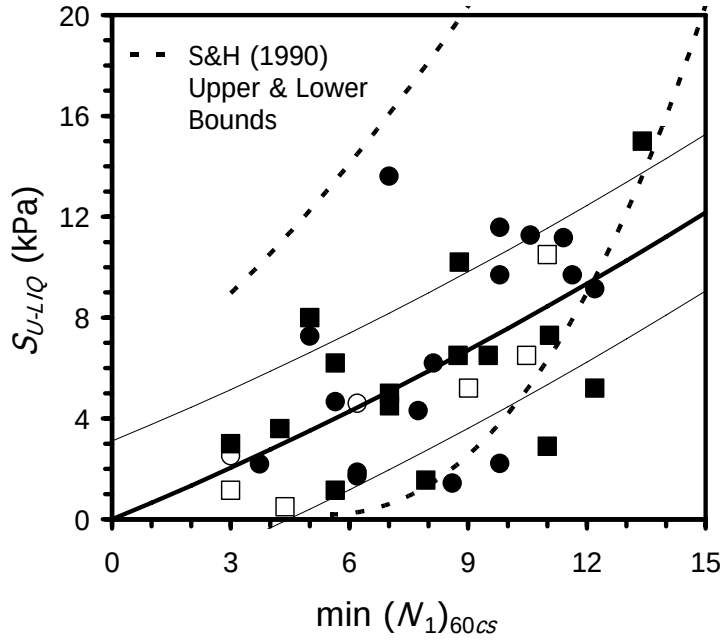

Figure 3-6 - Best-fit second-order polynomial regression for liquefied shear strength versus minimum SPT blow count corrected according to Youd et al. (2001) together with plus and minus one standard deviation lines (R^2 = 0.35).

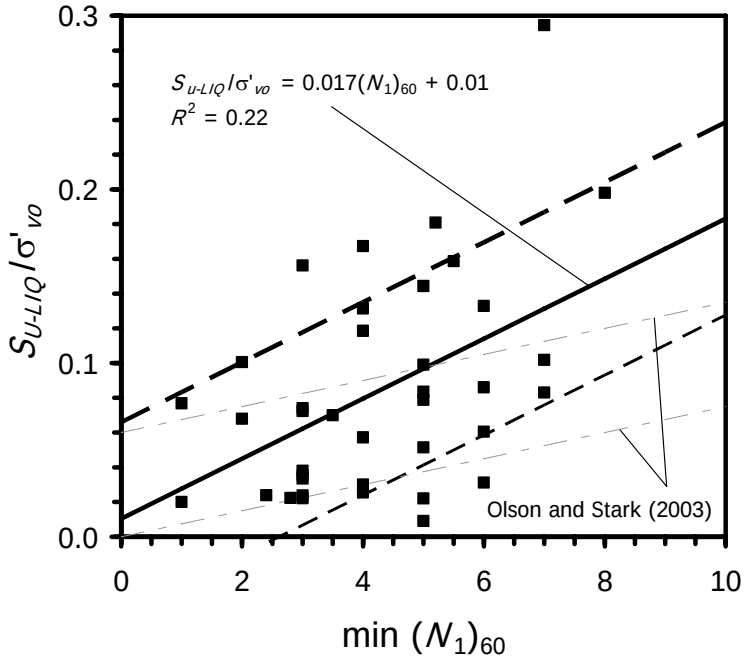

Figure 3-7- Best-fit linear regression for the normalized liquefied shear strength versus minimum SPT blow count together with plus and minus one standard deviation lines. The plus and minus one standard deviation lines presented by Olson and Stark (2003) are also included.

CHAPTER 4 - PROBABILISTIC ANALYSIS OF FLOW FAILURE CASES

Summary

This chapter presents the results of probabilistic analyses of the liquefied shear strength of liquefiable soils from field liquefaction case histories. The liquefied shear strength is the main parameter determining the post-liquefaction stability of natural slopes, and embankment dams and foundations, and whether a soil mass will experience flow failure or significant deformations. Based on a review of the literature and databases of flow liquefaction case histories, new cases of flow liquefaction were identified and included in existing databases. Using an advanced First-Order Reliability Methods (FORM), Monte Carlo Simulation (MCS), and Bayesian Mapping (BM), reliability-based back-analysis procedures are developed to provide rigorous methods for quantifying the reliability of liquefied shear strengths determined from case histories. Uncertainties in parameters needed to establish liquefied shear strengths and in the SPT-values are quantified and used to determine the reliability of the field data. Using the database of reliability estimates of the field data, probabilistic correlations between liquefied shear strength and SPT blow count are developed. The correlations are formulated to provide measures of flow liquefaction risk in terms of probability of failure, which could be used in conjunction with traditional factors of safety.

Introduction

The critical parameter involved in assessing and designing against the harmful effects of liquefaction is the liquefied shear strength, or the resistance available after liquefaction has occurred. While methods are available to determine the liquefied shear strength, they are based on limited data, utilize deterministic procedures, and do not provide sufficient details for

choosing appropriate strengths. Selection of the liquefied shear strength, $S_{u\text{-}LIQ}$, is an important decision because the chosen value can unnecessarily drive up repair/design costs or lead to the construction of unsafe structures.

The residual shear strength is the main factor determining the post-liquefaction stability of natural slope, and embankment dams and foundations, and whether a soil mass will experience flow failure or significant deformations. The cost and extent of measures required to ensure the stability of embankment dams against liquefaction are greatly influenced by the magnitude of the residual shear strength. As pointed out by Seed (1987), it may be adequate and economically advantageous simply to ensure the stability of an earth deposit or structure against flow failure after the strength loss due to liquefaction has been triggered than to prevent the triggering itself. Recent studies performed by the Association of State Dam Safety Officials, report that more than $30 billion are needed to rehabilitate or remove thousands of unsafe dams in the United States that may be susceptible to liquefaction-induce failure (ASCE, 2005). Before billions of dollars are spent on refurbishing or removing earthquake-prone dams and other civil works projects, procedures are needed to rationally select liquefied shear strengths for design and analysis.

The main objective of this paper is to present the application of probabilistic slope stability analysis to cases of liquefaction flow failure described in Chapter 3. This chapter describes the use of the First-Order Reliability Method (FORM) and Monte Carlo Simulations (FORM) to calculate probabilities of failure for cases of flow failure using the deterministic liquefied shear strength versus minimum SPT blow count relationship presented Chapter 3. Probabilistic liquefied shear strength criteria are developed from the results using a Bayesian Mapping technique. In addition, the spatial variability of the liquefied shear strength is

investigated to demonstrate how the spatial distribution of material properties can affect probability of failure estimates.

Case Histories and Methods of Stability Analysis

The 38 case histories of flow liquefaction examined in this chapter are presented in Table 3-1 of Chapter 3 where the methods of slope stability used to analyze the case histories are also discussed. The case histories are composed of 18 failures which are analyzed with the infinite slope model and 20 of which are analyzed with Spencer's (1967) method of slices. Figure 4-1 contains the best-fit second-order polynomial presented in Chapter 3 through the $S_{U\text{-}LIQ}$ vs. minimum $(N_1)_{60}$ data obtained from the deterministic back-analyses of the failures, along with lines corresponding to plus and minus one standard error of estimate, $S_{Y.X}$ (analogous to standard deviation). Table 4-2 shows the back-calculated mean and standard deviation values of $(N_1)_{60}$ and S_{u-LIQ} from case histories, while Table 4-3 gives the corresponding factors of safety and probabilities of failure with and without model correction C_1. The values given in Tables 4-2 and 4-3 used to generate Figures 4-1 and 4-2.

The deterministic *FS* for each case is computed using the mean input values and the appropriate slope stability model. The PDF of the minimum SPT blow counts $(N_1)_{60}$ for each case is used to compute the distribution of liquefied shear strength from the relationship presented in Figure 4-1. The post-failure geometries are used for the probabilistic analyses described in this chapter since the liquefied shear strength is mobilized in the post-failure geometry. When analyzing existing dams and slopes that have not failed, estimates of the post-failure geometry should be made prior to estimating the probability of P_F using liquefied shear strengths. As this is not the situation when analyzing actual failures, estimates of the post-failure

geometry, which are usually known, are not necessary. However, in cases where the post-failure geometry cannot be established, as in the case of predicting post-liquefaction deformations, several simple methods are available based on empirical correlations such as those described by Wride et al. (1999), and Hunter and Fell (2001). These methods use pre-failure geometrical dimensions, configurations, and soil properties to estimate post-failure geometries. The estimates are based on collections of varying slope failures from around the world. Additionally, more rigorous procedures using numerical models with the Finite Element Method (FEM) or the Finite Difference Method (FDM) can provide detailed estimates of the post-failure geometry. Several numerical modeling procedures are described by Seed and Harder (1990), Griffiths and Fenton (2004), and Ozutsumi et al. (2002) for estimating deformations and potential post-failure geometries.

Parameter Uncertainties

For all case histories, the magnitudes of uncertainties involved in evaluating the liquefied shear strength from field data have been carefully delineated and systematically analyzed. Probability distribution functions (PDF) representative of the various parameters involved in the stability analyses are developed through available data from each case history or from historical catalogs of parameter uncertainty. For those case histories where the variations in site-specific data are not available, published representative values of probabilistic parameters are used.

Normal and lognormal PDF's are two widely used distributions. While most data in nature appears to follow these distributions, they both can provide unreasonable values for geotechnical problems. The normal distribution spans from negative infinity to positive infinity. When modeling parameters such as shear strength, friction angle, or unit weight, negative and

very high positive values are not reasonable. The lognormal distribution spans from zero to positive infinity. While the lognormal PDF does avoids the problem with negative values, very high positive values approaching infinity can still lead to unrealistic results and numerical problems. In addition, for most geotechnical parameters lower bounds greater than zero are desirable. For example, the friction angle will likely never approach zero for drained sand in the field. To address the shortcomings of both normal and lognormal distributions, the Beta distribution is employed. The Beta distribution is defined with four parameters: α, β, minimum, and maximum. The mean μ and standard deviation σ of the Beta distribution can be computed with the following equations:

$$\mu = \min + \frac{\alpha}{\alpha+\beta}(\max - \min) \tag{4-1}$$

$$\sigma = \sqrt{\frac{\alpha\beta}{(\alpha+\beta)^2(\alpha+\beta+1)}(\max - \min)^2} \tag{4-2}$$

Eqs. (4-1) and (6-2) can be used to estimate values of α and β for the Beta distribution. The mean and standard deviation for a particular parameter can be estimated from actual data or from published values along with typical coefficients of variation *COV*, where $COV = \sigma / \mu$. With an estimated μ and σ, the minimum and maximum values can be estimated as plus and minus three standard deviations from the mean. Setting up a simple optimization problem, the α and β parameters can be varied until the Eqs. (4-1) and (4-2) are equal to the μ and σ of the particular parameter. The Beta probability distribution function is very flexible with the ability to adapt to almost any distribution of data.

For the cases analyzed with the infinite slope model, the depth to the water table H_d is estimated from the results of borings and local ground conditions. The height of water above the

ground surface $H_w$is determined by measuring depths from the top of the water table to the top and bottom of the presumed liquefiable soil deposit. Post-failure cross-sections, surveys, and measured displacements are used to assess the variability in the slope angle α from each case. Table 4-1 presents the *COV* values for the input parameters used in analyzing the infinite slope case histories.

For cases analyzed with Spencer's method, laboratory and field data from pre- and post-failure surveys are used to quantify parameter uncertainties. Investigation of the *COV*s for input parameters involved in the complex case histories are typically less than 10%. To account for unforeseen uncertainties in the input parameters, a conservative *COV* of 10% is used to model the uncertainty in all the parameter. The *COV* for minimum SPT blow counts is assigned a value of 30% which is consistent with studies on the uncertainty involved with SPT testing.

It is often the case that material properties are correlated, and this correlation can be modeled with a correlation matrix. For instance, the dry and saturated unit weights of soils are expected to be correlated. The correlation matrix consists of the correlation coefficients ρ for all parameters involved in probabilistic calculations. The correlation coefficient ρ_{xy} between two points *x* and *y* is given as:

$$\rho_{xy} = \frac{\frac{1}{n}\sum_{i=1}^{n}\left(X_i - \mu_x\right)\left(Y_i - \mu_y\right)}{\sigma_x \cdot \sigma_y} \tag{4-3}$$

where *n* is the number of samples, X_i and Y_i are vectors of variable *x* and *y*, μ_x and μ_y are mean values, and σ_x and σ_y are standard deviations of the vectors, X_i and Y_i. For the analyses described below, the material properties in the different soil zones are assumed to be uncorrelated, that is, the correlation coefficients amongst the input parameters are assigned a value of zero. For

material properties within the same soil zone, each property is assumed to be perfectly correlated with a value of one.

Probabilistic Procedures

The First-Order Reliability Method (FORM), and Monte Carlo Simulation (MCS) are used to estimate the probability of failure P_F for the cases of flow liquefaction failure. These probabilistic procedures were presented and discussed with respect to the infinite slope stability cases presented in Chapter 3. The effects of autocorrelation distance on the probability of failure are thoroughly discussed by Ang and Tang (1975, 1990), and Baecher and Christian (2003).

Calculation of failure probability requires definition of a performance function. Performance functions provide the limit surface which defines the boundary between failure and safety. Typically, failure is defined as factors of safety less than one, and safety is defined as factors of safety greater than one. Therefore, the performance function $G(x)$ used to assess the reliability is given as:

$$G(x) = C_1 FS - 1 \tag{4-4}$$

where the factor of safety FS is a function of all parameters involved in the slope stability analysis including the liquefied shear strength. The term C_1 accounts for uncertainty in the performance function and is discussed in more detail in a subsequent section. Failure corresponds to $G(x) \leq 0$ and safety corresponds to $G(x) > 0$.

First-Order Reliability Method

FORM involves calculation of the reliability index β, which is a measure of the standardized distance between the "mean" point (all inputs are assigned mean values) and the failure surface or limit state. Eq. (4-5) is used to calculate the reliability index β:

$$\beta = \min_{\underline{x} \in F} \sqrt{\left[\frac{x_i - m_i^N}{\sigma_i^N}\right]^T \left[\underline{R}\right]^{-1} \left[\frac{x_i - m_i^N}{\sigma_i^N}\right]} \tag{4-5}$$

where $\underline{x}$ is a vector representing the random variables in the slope stability calculations, F is the failure domain, $[R]$ is the correlation matrix (the correlation matrix is composed of the terms ρ_{xy} as shown in Eq. 4-3), and m_i^N and σ_i^N are vectors of the equivalent-normal mean and standard deviation computed from Rackwitz-Fiessler (1978) transformations. Several procedures are available to compute β most of which involve developing the first derivative of the performance function. This task can be quite cumbersome as the performance function becomes complex. Low and Tang (2004) present an ellipsoidal approach where formulation of the first derivative is not required, and allows for the easy incorporation of correlated and non-normal parameters in a spreadsheet format. When calculating reliability indices using Eq. (4-5), it is important to consider the sign of the deterministic factor of safety *FS* as only positive values of β can be obtained. If the deterministic *FS* is less than one (i.e. within the failure domain) the computed reliability index should be made negative. If the deterministic *FS* is greater than one (i.e. with the safe domain), then the computed reliability index should be positive.

The probability of failure P_F is normally computed with the notional probability concept, which assumes that P_F can be computed from the reliability index β according to:

$$P_F = 1 - \Phi(\beta) = \Phi(-\beta) \tag{4-6}$$

where Φ() is the cumulative normal distribution.

Monte Carlo Simulations

Monte Carlo Simulations consist of generating a large number of samples, typically on the order of 10,000 to 100,000, from probability density functions and calculating the performance function for each group of samples using a prescribed stability model. Several commercially available software packages, such as the Excel™ add-in software @RISK™ (Palisades, 1996), can be used to perform the simulations. In addition, the slope stability software SLIDE 5.0 from Rocscience (2006) combines MCS with several stability models. SLIDE 5.0 is used to analyze the Spencer-type cases of slope instability, while the infinite slope cases were analyzed using implementations of FORM and MCS in Excel and @RISK. In the context of slope stability, MCS provides a distribution of the factor of safety. The probability of failure is computed as the area under the factor of safety probability density function less than one, or in other words the probability that the performance function (Eq. 4-4) is less than zero. When the MCS and FORM models are setup in the same manner, the estimated P_F values are nearly identical as shown by Low and Tang (1997) and in Chapter 3 where both MCS and FORM were shown to yield identical P_F values for the infinite slope analyses.

Spatial Variability

Soil properties almost always vary from point to point with a soil deposit. Oftentimes this variability is ignored by using average material properties to model an entire deposit. Techniques are available to quantitatively account for the variability of material properties throughout a soil deposit. Autocorrelation functions are used to construct the correlation matrix based on calculated distances between different points within the slope stability cross-section. Griffiths and Fenton (2004) combine autocorrelation functions with the Finite Element Method to model

spatial variability in slopes. The exponential autocorrelation model is shown in the Eq. (4-7) is commonly used to model the spatial variability of material properties:

$$\rho_{xy} = \exp\left(-\delta / \delta_0\right) \tag{4-7}$$

where δ is the distance between two points, and δ_0 is the autocorrelation distance. The correlation matrix is constructed with Eq. (4-7) for the spatially correlated material properties. Autocorrelation distances can be estimated for different material properties through the analysis of spatial data. Correlation coefficients are calculated for different separation distances, and the autocorrelation distance is estimated by fitting the autocorrelation function Eq. (4-7) to the data.

Horizontal and vertical autocorrelation distances should be analyzed when accounting for spatial variability. Autocorrelation distances are typically larger in the horizontal direction as compared to the vertical direction as a result of layering caused by geologic processes and, in the case of hydraulically built earth embankments, by the construction processes. For example, material properties are likely to be similar within a particular soil deposit at the same elevation over considerable distances. Whereas, the material properties at different elevations within a soil deposit will likely vary over shorter distances. Appropriate δ_0 values should be chosen to represent material variability in the horizontal or vertical directions.

Probabilities of Failure from Case Histories

In order to develop a probabilistic relationship between the liquefied shear strength $S_{U\text{-}LIQ}$ vs. and minimum SPT blow count $(N_1)_{60}$, it is necessary to develop a relationship between factor of safety *FS* and probability of failure *PF*. The deterministic factors of safety *FS* and probabilities of failure P_F for each of the post-liquefaction case histories listed in Table 4.2 are mapped using

a Bayesian Mapping (BM) technique described by Juang et al. (2006). The BM procedure is based on regression analyses with the logistic function of the form:

$$P_F = \frac{1}{1+\left(FS/A\right)^B} \tag{4-8}$$

where A and B are mapping coefficients. This mapping function has been used by past researchers to successfully establish relations between factors of safety and probabilities of liquefaction for liquefaction potential evaluations (e.g., Juang et al. 2002, and Juang et al. 2006). Figure 4-3 contains a plot of deterministic factor of safety versus probability of failure for the flow failure cases presented in Table 4-1 without consideration for model uncertainty. This figure also contains a relationship between FS and P_F obtained through a least-square fit using Eq. (4-8). Figure 4-3 shows that the probability of failure decreases as the deterministic factor of safety increases, which is expected.

Model Uncertainty

Incorporating performance function uncertainties with the C_1 term shown in Eq. (4-4) provides a more rigorous approach to computing the probability of failure. As discussed by Juang et al. (2006), if model uncertainties are not accounted for, the computed P_F values may be inaccurate. In order to assess the model uncertainty term C_1, parametric studies are performed by changing the mean (μ_{C1}) and standard deviation (σ_{C1}) of C_1, which is assumed to be normally distributed. The process used to determine the distribution parameters for C_1 is shown in Figure 4-4 as a flowchart. The values of μ_{C1} and σ_{C1} are varied until the P_F computed from the FORM or MCS match those calculated from the PDF of the reliability index. The P_F values computed for the case histories analyzed with Spencer's method are converted to reliability indices using Eq. (4-6). The values are matched such that the FORM and MCS are calibrated to the reliability index PDF.

Figure 4-5 presents probabilities of failure for the case histories computed from the PDF of reliability indices as a function of deterministic *FS*. The model uncertainty term C_1 is determined assuming that the PDF of the reliability index β captures the uncertainty in the relationship between factor of safety and probability of flow failure. Figure 4-6 presents probabilities of failure computed with the C_1 term as a function of *FS*. Based on these parametric studies, the model uncertainty term has a μ of 1.0 and σ of 0.4.

When data is available for characterizing parameter uncertainties, probabilities of failure should be computed which incorporate the model uncertainty term in the performance function. In those cases where insufficient data is available or a quick screening is desired, deterministic factors of safety can be computed and probabilities estimated based on the Bayesian Mapping functions described above.

Probabilistic Liquefied Shear Strength Criteria

Eq. (4-7) can be rewritten so as to plot contours of the probability of P_F on a $S_{u\text{-}LIQ}(FFD)$ vs. $(N_1)_{60}$ plot and to establish a relationship of the form:

$$\frac{S_u\left[(N_1)_{60}\right]}{FFD} = A\left(\frac{1}{P_F} - 1\right)^{1/B} \tag{4-9}$$

where $S_u\left[(N_1)_{60}\right]$ is the liquefied shear strength from the relationship shown in Figure 4-1, and *FFD* is the flow failure demand, which is the shear stress acting on the post-failure geometry of failed slope. The parameter *FFD* is analogous to the parameter *CSR* (cyclic shear stress ratio) used in the "simplified procedure" for liquefaction evaluation (Youd et al. 2001). The *FFD* can be estimated from the slope stability models described in the companion paper.

Probabilistic $S_{U\text{-}LIQ}$ versus minimum $(N_1)_{60}$ criteria are presented in Figure 4-7 containing P_F contours corresponding to 2%, 16%, and 50%. As can be seen, the P_F=50% curve coincides

very closely to the best-fit second-order polynomial function through the data points. Also, the P_F=2% curve appears to be the lowest probability of failure as almost all points lie above this curve. Figure 4-8 can be used in three ways to perform quick and simple analyses of slopes and dams containing potentially liquefiable soils, namely: 1) with a minimum SPT blow count and the *FFD* the P_F can be estimated, 2) with a minimum SPT and a desired P_F the corresponding *FFD* can be estimated, and 3) with the PDF of the minimum SPT, the distribution of the liquefied shear strength can be estimated for use in probabilistic slope stability calculations.

The authors' recommend performing a rigorous probabilistic analysis using the FORM or MCS including the model uncertainty term discussed in the previous section. Figures 4-6 and 4-7 can provide a preliminary estimate of the P_F, however, specific uncertainties at each site may affect the estimates. When sufficient data is available, spatial variability should also be accounted for as the computed P_F values may increase or decrease. Figure 4-7 may be used to arrive at a preliminary estimate of the effect of the correlation distance δ_0 on the probability of failure.

The lines shown in Figure 4-7, which correspond to probabilities of failure (P_F) equal to 2%, 16%, and 50%, are the curves of flow failure demand (*FFD*) necessary to produce that particular probability of failure using the curve of liquefied shear strength on the plot. In other words, with the liquefied shear strength ($S_{u\text{-}LIQ}$) estimated from the average trend line the flow failure demand (or driving stress) required to produce a particular probability of failure would be calculated from the corresponding equation/curve. The general equation for the *FFD* is as follows (where *FFD* will be computed in units of kPa):

$$FFD = \frac{0.87\min\left(N_1\right)_{60} + 0.1\left(\min\left(N_1\right)_{60}\right)^2}{1+\left(\frac{1-P_F}{P_F}\right)^{\left(1/2.908\right)}} \tag{4-10}$$

For example, let's say we have a potentially liquefiable stratum with a $\min(N_1)_{60}$ blow count of 6 bpf and we want our design to have 2% probability of failure. Plugging the two values into the above equation leads to a *FFD* equal to 2.21 kPa (the $S_{u\text{-}LIQ}$ would be 8.82 kPa), if the actual *FFD* on the slip surface is greater than 2.21 kPa then the P_F would be higher than 2% and if the actual *FFD* on the slip surface is less than 2.21 kPa then the P_F would be lower than 2%.

The equations for the curves shown in Figure 4-7 are as follows:

For the average $S_{u\text{-}LIQ}$:

$$S_{U-LIQ} = 0.87\min(N_1)_{60} + 0.1(\min(N_1)_{60})^2 \tag{4-11}$$

For P_F = 2%:

$$FFD = \left(\frac{1}{4}\right)\left[0.87\min(N_1)_{60} + 0.1(\min(N_1)_{60})^2\right] \tag{4-12}$$

For P_F = 16%:

$$FFD = \left(\frac{1}{1.85}\right)\left[0.87\min(N_1)_{60} + 0.1(\min(N_1)_{60})^2\right] \tag{4-13}$$

For P_F = 50%:

$$FFD = \left(\frac{1}{1.048}\right)\left[0.87\min(N_1)_{60} + 0.1(\min(N_1)_{60})^2\right] \tag{4-14}$$

The other way to use the sets of equations would be to estimate the *FFD* on the slip surface using slope stability calculations and estimate the $\min(N_1)_{60}$ blow count along the slip surface. Rearranging Eq. (4.11) and solving for P_F leads to the following equation:

$$P_F = \frac{1}{1+\left(\frac{0.87\min(N_1)_{60} + 0.1(\min(N_1)_{60})^2}{1.048FFD}\right)^{2.908}} \tag{4-15}$$

Using the same values as before let's say the min$(N_1)_{60}$ blow count is 6 and the estimated *FFD* is 2.21 kPa, plugging these values into the previous equation leads to a computed P_F equal to 2%.

Conclusions and Recommendations

The following list contains pertinent conclusions and recommendations on SPT-based the probabilistic liquefied shear strength criterion derived in this chapter:

1. Several probabilistic procedures, including the First-Order Reliability Method and Monte Carlo Simulations are used in combination limit equilibrium methods to analyze case histories of flow failure presented in Chapter 3.
2. The Beta probability density function is suitable for modeling of the statistical variability of the geotechnical parameters as the distribution can be truncated with minimum and maximum values. Estimates of parameter means and *COV* values can easily be represented with a Beta PDF.
3. Implementing a Bayesian Mapping procedure, values of P_F are computed from the probability density function of the reliability indices of flow failure. The mapping function is obtained relating the deterministic factor of safety to P_F for the liquefied shear strength relationship presented in Figure 4-1. The P_F can be computed using the BM equation and the deterministic factor of safety, computed with mean or average values.
4. When the deterministic *FS* is equal to unity, spatial variability of the material properties does not affect computed probabilities of failure. Therefore, spatial variability does not affect back-calculated liquefied shear strength from case histories as the *FS* is unity. If the deterministic *FS* is greater than one, accounting for spatial variability will decrease

the estimated P_F. Conversely, if the deterministic FS is less than one, accounting for spatial variability will increase the estimate P_F.

5. Charts were developed based on Bayesian Mapping of the case histories which provide several methods for screening soil slopes or dams containing liquefiable soils. The charts require two of three inputs for use, minimum $(N_1)_{60}$ blow count, flow failure demand FFD, or probability of flow P_F.
6. Without accounting for uncertainty in the performance function, probabilities of failure computed from the FORM or MCS may be inaccurate. It is shown that through an iterative procedure the mean and standard deviation of the model uncertainty term, C_1, can be estimated. The model uncertainty for the liquefied shear strength relationship presented in Figure 4-1 has a mean of 1.0 and standard deviation of 0.4, resulting in a COV of 40%.
7. The author's recommend performing probabilistic analyses with either the infinite slope model or Spencer's (1967) method of slices, depending on geometry, along with PDF's to model various input parameters.

Chapter 4 References

ASCE (2006). " American Society of Civil Engineering 2005 Report Card," <www.asce.org/reportcard>.

Ang, A. and Tang, W.H. (1975). *Probability Concepts in Engineering Planning and Design: Volume I - Basic Principles*. John Wiley and Sons, Ltd., New York

Ang, A. and Tang, W.H. (1990). *Probability Concepts in Engineering Planning and Design: Volume II - Design, Risk, and Reliability*. Copyrighted by Authors.

Baecher, G.B. and Christian, J.T. Reliability and Statistics in Geotechnical Engineering. John Wiley and Sons, Ltd., New York

Eddy, M.A., Gutierrez, M.S., and Snorteland, N. (2006). "Probabilistic liquefied shear strength from in situ test data." *J. Geotech. Geoenvir. Eng., ASCE.* (In review).

Griffiths, D.V. and Fenton, G.A. (2004). "Probabilistic Slope Stability Analysis by Finite Elements." *J. Geotech. Geoenvir. Eng., ASCE.* 130(5): 507-518.

Juang, C.H., Fang, S.Y., and Khor, E.H. (2006). "First-order Reliability Method for Probabilistic Liquefaction triggering Analysis using CPT." *J. Geotech. Geoenvir. Eng., ASCE.* 132(3): 337-350.

Juang, C.H., Jiang, T. and R.D. Andrus (2002). "Assessing probability-based methods for liquefaction potential evaluation." *J. Geotech. Geoenvir. Eng., ASCE*, 128(7), 580-589.

Low, B.K. and Tang, W.H. (1997). "Reliability analysis of reinforced embankments on soft ground." *Canadian Geotech. Journal*., 34: 672-685.

Low, B.K. and Tang, W.H. (2004). "Reliability analysis using object-oriented constrained optimization," *Structural Safety*, vol. 26: 69-89.

National Oceanic and Atmospheric Administration (NOAA), (2006). United States Department of Commerce. <http://www.ngdc.noaa.gov/seg/hazard/sig_srch_idb.shtml>

Ozutsumi, O., Sawada, S., Takeshima, Y., Sugiyami, W., and Shimazu, T. (2002). "Effective stress analyses of liquefaction-induced deformation in river dikes." *Soil Dynamics and Earthquake Engineering*, vol. 22: 1075-1082.

Palisade Corporation. (1996). "@RISK: Risk analysis and simulation add-in for Microsoft Excel or Lotus 1-2-3." Palisade Corporation, Newfield, N.Y.

Rackwitz, R. and Fiessler, B. (1978). "Structural reliability under combined random load sequences." *Comp. Struct.*, 9, 484–494.

Rocscience, Inc. (2006). "SLIDE version 5.025: 2-D Limit Equilibrium Analysis of Slope Stability." Rocscience, Inc., Toronto, Ontario.

Spencer, E. (1967). "A method of analysis of the stability of embankments assuming parallel interslice forces." *Géotechnique*, London, 17(1), 11-26.

Wride (Fear), C.E., McRoberts, E.C. and Robertson, P.K. (1999). "Reconsideration of case histories for estimating undrained shear strength in sandy soils." *Can. Geotech. J.*, 36, 907-933.

Chapter 4 Tables

Table 4-1 - Coefficients of Variation, *COV*, (%) for input parameters involved in analysis of infinite slope case histories.

ID #	H_w, m	H_d, m	γ_{sat}, kN/m^3	γ_m, kN/m^3	α, °	min $(N_1)_{60}$
2	30.0	10.0	5.0	5.0	10.0	20.0
4	30.0	10.0	5.0	5.0	11.6	5.0
5	29.4	10.0	5.0	5.0	10.0	23.8
6	16.5	0.0	1.9	-	8.3	17.0
7	30.0	10.0	5.0	5.0	10.0	35.0
10	6.7	10.0	10.0	10.0	6.7	33.3
11	11.0	0.0	10.2	-	3.8	10.0
12	30.0	10.0	5.0	5.0	10.0	43.4
13	14.3	0.0	10.0	-	21.7	16.0
22	33.5	0.0	10.0	-	16.8	11.0
23	17.5	0.0	10.0	-	4.1	25.0
24	17.5	0.0	10.0	-	3.4	25.0
26	9.7	0.0	10.0	-	2.5	14.0
27	28.6	0.0	10.0	-	2.1	10.0
28	10.0	10.0	10.0	10.0	2.1	14.3
29	8.6	10.7	10.0	10.0	22.2	21.7
30	30.0	10.0	5.0	5.0	10.0	33.3
34	3.7	0.0	10.0	-	4.3	26.1

Table 4-2 – Back-calculated mean and standard deviation values of $(N_1)_{60}$ and S_{u-LIQ} from case histories.

ID #	Case History	$(N_1)_{60}$		$S_{U\text{-}LIQ}$ (kPa)	
		μ	σ	μ	σ
1	Calaveras Dam	5.0	1.50	6.5	
2	Cark Canal	3.0	0.60	1.4	0.20
3	Chonan Middle School	5.2	1.56	10.2	0.78
4	Cumhuriyet	4.0	0.20	2.2	0.55
5	Degirmendere Nose	8.0	1.90	11.2	1.70
6	El Cobre Tailings Dam	1.0	0.17	1.9	0.35
7	Esme Nose	6.0	2.10	9.2	2.53
8	Fort Peck Dam	5.0	1.50	2.9	
9	Hachiro-Gato Roadway Embankment	3.0	0.90	1.2	
10	Heber Road	3.0	1.00	1.7	0.20
11	Hokkaido Tailings Dam	1.0	0.10	4.6	0.72
12	Hotel Sapanca	2.8	1.20	2.2	0.58
13	Itoizawa Road Fill	5.0	0.80	7.3	2.02
14	Koda Numa Highway Embankment	2.4	0.72	0.5	
15	La Marquesa Dam (Downstream)	5.5	1.65	7.3	0.35
16	La Marquesa Dam (Upstream)	4.0	1.20	1.6	
17	La Palma Dam	3.0	0.90	6.2	
18	Lake Ackerman Roadway Embankment	3.0	0.90	3.0	
19	Lake Merced Bank	5.0	1.50	8.0	
20	Lower San Fernando Dam	6.0	1.80	5.2	
21	May 1 Slide	5.0	1.50	10.5	
22	Metoki Road Embankment	3.0	0.33	2.5	0.98
23	Mochikoshi Dike 1	4.0	1.00	9.7	2.00
24	Mochikoshi Dike 2	4.0	1.00	11.6	2.37
25	Nalband Railway Embankment	6.0	1.80	6.5	
26	Niteko Middle Dam	3.0	0.70	4.7	1.42
27	Niteko Upper Dam	5.0	0.30	4.3	0.61
28	River Park	7.0	1.00	13.6	1.35
29	Route 272	4.0	1.30	6.2	1.50
30	Seyman Tea Garden	6.0	2.00	9.7	2.85
31	Shibecha-Cho Embankment	5.0	1.50	5.2	0.54
32	Shiribeshi-Toshibetsu Site 3	2.0	0.60	4.5	
33	Shiribeshi-Toshibetsu Site 5	2.0	0.60	5.0	
34	Tar Island Dyke	7.0	1.83	11.3	1.30
35	Uetsu-Line Railway Embankment	3.0	0.90	1.2	0.14
36	Upper San Fernando Dam	7.0	2.10	15.0	
37	Wachusett Dam (North Dike)	4.0	1.20	3.6	
38	Yodo Site 6	3.5	1.05	6.5	

Table 4-3 – Factors of safety and probabilities of failure from case histories with and without model correction.

#	Case History	*FS*	P_F		
			w/o C_1	β PDF	w/ C_1
1	Calaveras Dam	1.06	44.71%	50.74%	50.54%
2	Cark Canal	0.96	54.55%	56.33%	53.19%
3	Chonan Middle School	0.83	65.63%	62.64%	57.44%
4	Cumhuriyet	0.50	99.97%	96.49%	96.51%
5	Degirmendere Nose	0.02	99.99%	99.99%	100.00%
6	El Cobre Tailings Dam	1.36	13.20%	29.61%	28.07%
7	Esme Nose	0.31	99.95%	95.87%	98.99%
8	Fort Peck Dam	1.98	0.16%	7.31%	14.12%
9	Hachiro-Gato Roadway Embankment	1.82	1.35%	13.46%	17.69%
10	Heber Road	0.26	100.00%	97.92%	99.71%
11	Hokkaido Tailings Dam	1.98	10.13%	26.73%	15.58%
12	Hotel Sapanca	0.79	85.34%	75.16%	70.53%
13	Itoizawa Road Fill	0.92	59.90%	59.36%	56.43%
14	Koda Numa Highway Embankment	2.98	0.03%	4.87%	6.27%
15	La Marquesa Dam (Downstream)	1.07	43.56%	50.08%	50.35%
16	La Marquesa Dam (Upstream)	2.25	2.01%	15.24%	13.30%
17	La Palma Dam	0.73	95.31%	84.22%	77.41%
18	Lake Ackerman Roadway Embankment	1.16	37.51%	46.53%	46.44%
19	Lake Merced Bank	0.91	70.41%	65.44%	66.56%
20	Lower San Fernando Dam	1.20	18.62%	34.05%	38.57%
21	May 1 Slide	0.99	49.70%	53.59%	52.75%
22	Metoki Road Embankment	1.55	3.33%	17.97%	20.23%
23	Mochikoshi Dike 1	0.73	93.18%	81.84%	77.58%
24	Mochikoshi Dike 2	2.38	0.70%	11.04%	8.46%
25	Nalband Railway Embankment	1.30	26.47%	39.61%	37.95%
26	Niteko Middle Dam	2.58	0.44%	9.68%	7.18%
27	Niteko Upper Dam	1.17	34.29%	44.59%	38.93%
28	River Park	0.94	54.03%	56.04%	53.29%
29	Route 272	1.40	19.99%	35.08%	28.33%
30	Seyman Tea Garden	1.43	29.06%	41.31%	31.90%
31	Shibecha-Cho Embankment	1.19	27.94%	40.58%	41.11%
32	Shiribeshi-Toshibetsu Site 3	0.82	85.51%	75.28%	69.82%
33	Shiribeshi-Toshibetsu Site 5	0.82	71.50%	66.10%	62.06%
34	Tar Island Dyke	0.86	60.67%	59.79%	58.68%
35	Uetsu-Line Railway Embankment	2.03	1.73%	14.52%	15.08%
36	Upper San Fernando Dam	0.84	78.10%	70.19%	67.32%
37	Wachusett Dam (North Dike)	1.29	22.38%	36.81%	36.59%
38	Yodo Site 6	0.81	83.65%	73.93%	71.75%

Chapter 4 Figures:

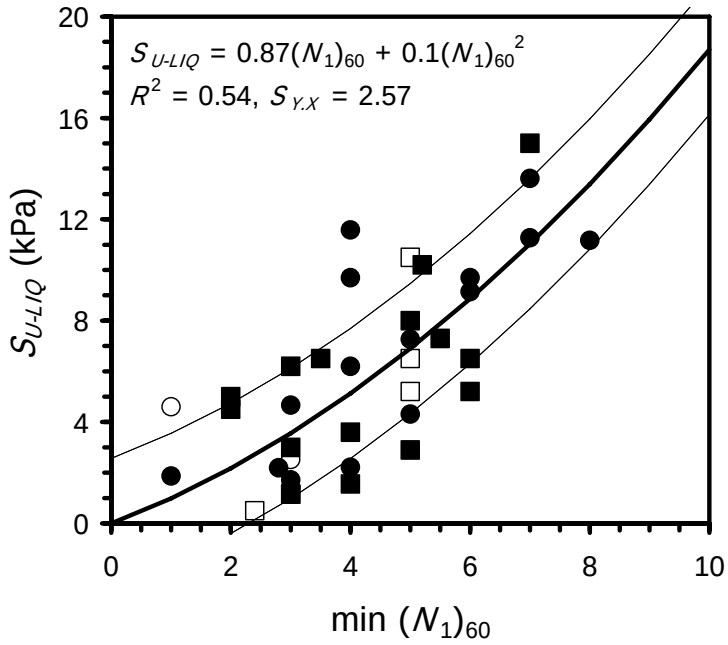

Figure 4-1 - Liquefied shear strength relationship from Chapter 3. Squares correspond to cases analyzed with Spencer's method and circles correspond to infinite slope cases. Solid symbols indicate that SPT data was measured at the site and open symbols indicate that SPT data was estimated.

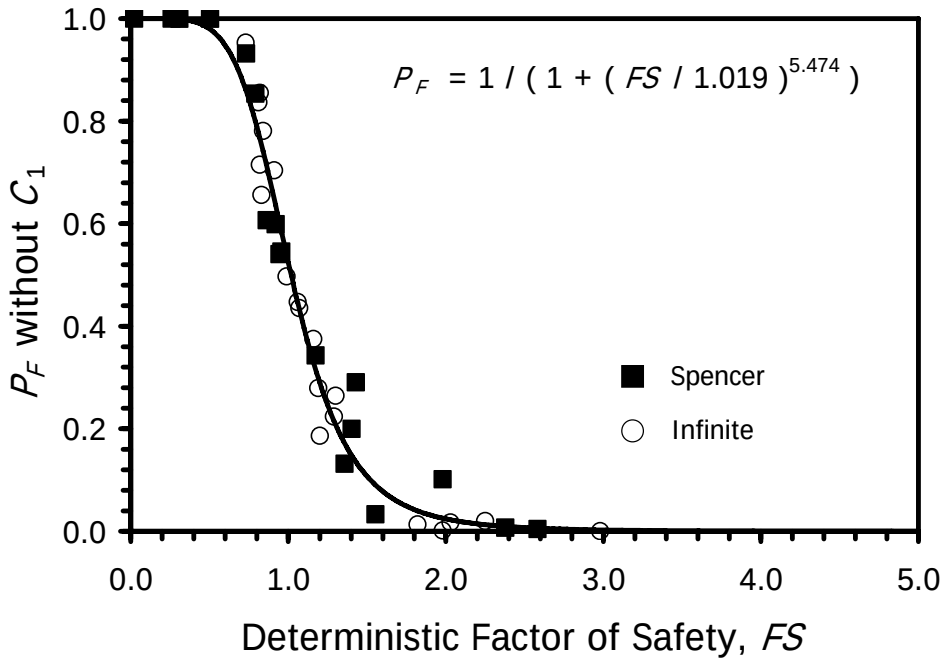

Figure 4-3 – Relationship between factor of safety *FS* and probability of failure P_F i considering the model uncertainty term C_1 ($\mu = 1.0$ and $\sigma = 0.0$).

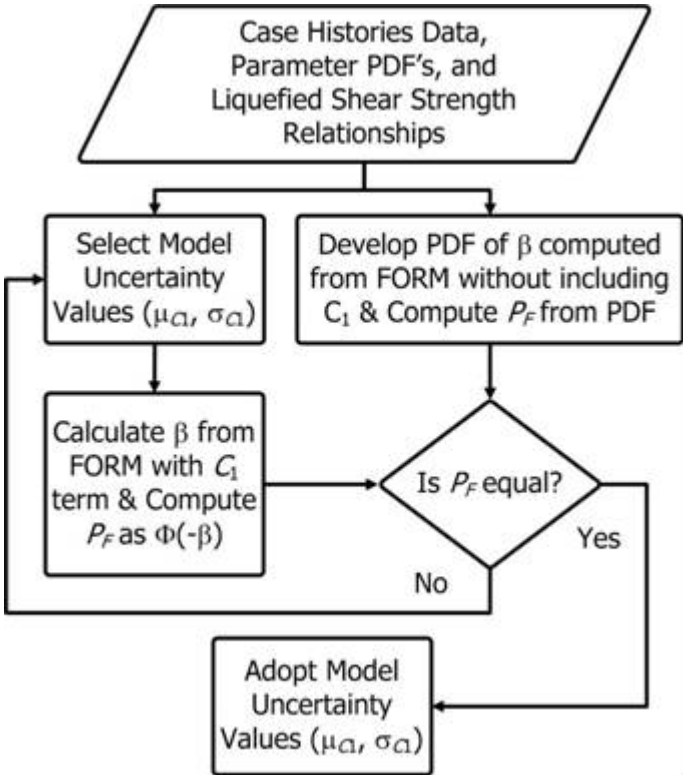

Figure 4-4 – Flowchart illustrating how the PDF parameters for the model uncertainty term, C_1, are determined through an iterative procedure.

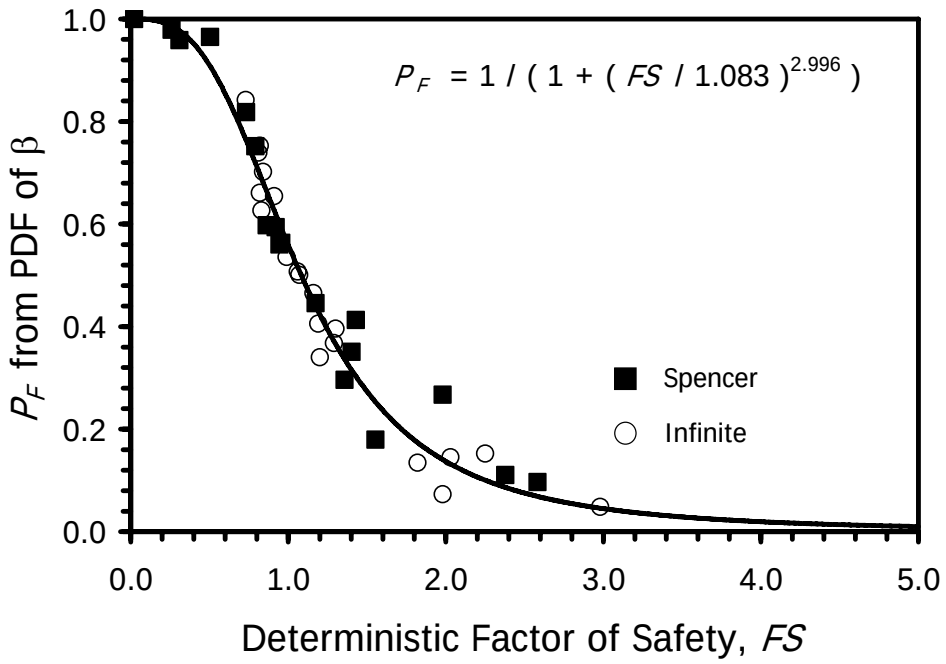

Figure 4-5 - P_F is computed from the PDF of the reliability indices without C_1. The reliability indices follow a logistic distribution with parameters ($\alpha = 0.166$, $\beta = 1.1$).

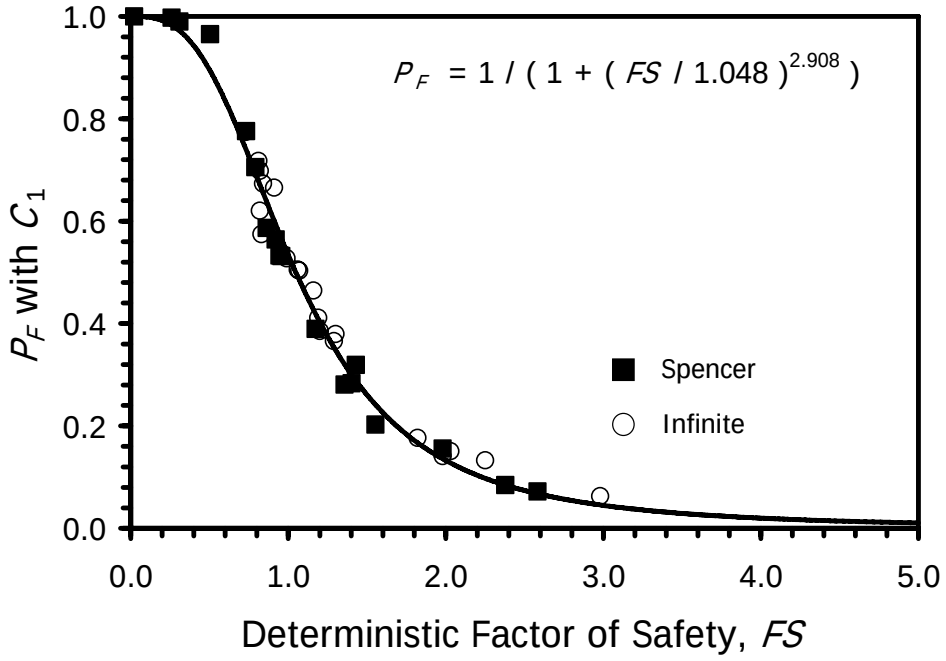

Figure 4-6 - Relationship between factor of safety *FS* and probability of failure P_F considering the model uncertainty term C_1 with μ =1.0 and σ= 0.4.

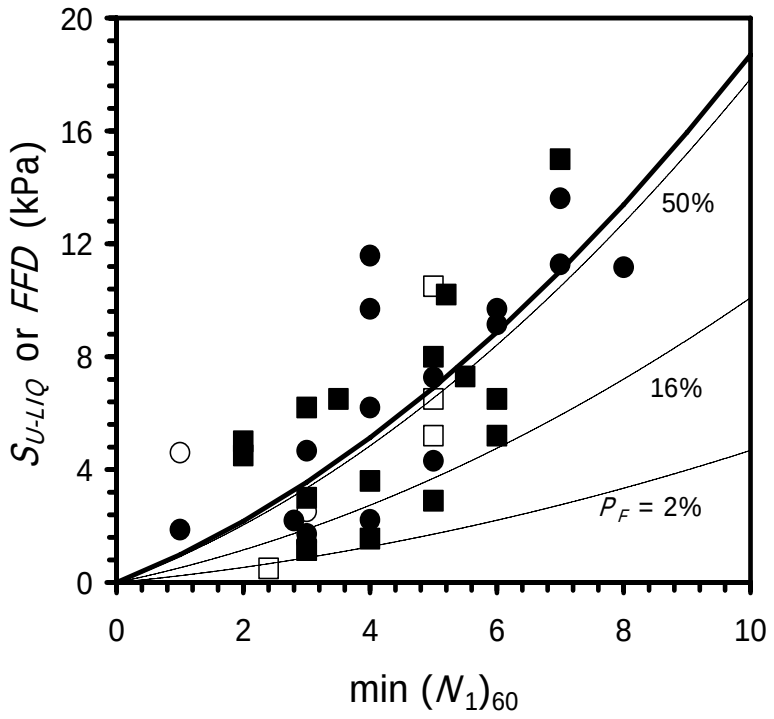

Figure 4-7 - Contours of P_F computed with the liquefied shear strength relation shown in Figure 4-1 including model uncertainty.

CHAPTER 5 - SUMMARY, CONCLUSIONS AND RECOMMENDATIONS

The general conclusions drawn from each chapter are presented here to summarize the findings of the research.

1) First Order Reliability Method (FORM) and Monte Carlo Simulation (MCS) can be used to perform a probabilistic back-analysis of the $S_{u\text{-}LIQ}$ from liquefaction flow failures. The probabilistic back-analysis provides a distribution of $S_{u\text{-}LIQ}$ for specific cases of flow failures by accounting for uncertainties in stability parameters. The results are then used to develop a flow failure criterion in terms of SPT blow count and $S_{u\text{-}LIQ}$.
2) The FORM and MCS are used to compute probabilities of flow failure based on three strength criterion: mean, and lower and upper bound. Results show that the P_F values determined from FORM and MCS are nearly identical. As the FORM method is computationally faster than the MCS, if possible FORM should be used in place of MCS for reliability calculations.
3) Implementing a Bayesian Mapping (BM) procedure, values of P_F are computed from the probability density functions of the reliability indices of flow failure. The PDF of β are different for different liquefied shear strength vs. SPT blow count relationship, and the mapping functions are obtained relating the deterministic factor of safety to P_F for each strength relationship. The P_F can be computed using the BM equation and the deterministic factor of safety, computed with mean or average values.
4) Reliability computations using an infinite slope stability model of 22 case histories with the upper, mean and lower strength criterion indicate that the upper and mean states predict low probabilities of flow failure ranging from 5 to 20% for some of the cases,

whereas the lower strength relationship predicts higher probabilities of flow failure greater than 30%.

5) Charts were developed based on BM of the case histories which provide several methods for screening soil slopes containing liquefiable soils. The charts require two of three inputs for use, minimum $(N_1)_{60}$ blow count, flow failure demand *FFD*, or probability of flow failure P_F.

6) Without accounting for uncertainty in the limit state model, reliability indices and probabilities of failure computed from the FORM may be inaccurate. It is shown that through an iterative procedure, the mean and standard deviation of the model uncertainty parameter C_1 can be obtained.

7) The authors' recommend the use of the lower bound liquefied shear strength vs. SPT blow count relationship for computing factors of safety and probabilities of flow failure. This recommendation appears to provide reasonable values of the probability of flow failure of about 20%. This value is consistent with 15-20% probability of liquefaction which is considered to be as acceptable risk in design of structures (Moss 2003, Juang et al. 2006). On other hand, the mean and upper bound liquefied shear strength vs. SPT blow count relationships give very high values of probability of flow failure of 55% and 85%, respectively. More research is needed to judge the appropriate level of probability of failure in terms of allowable risk and consequences of flow failure.

8) Cases analyzed with an infinite slope model and the Spencer's generalized method of slices can be combined to develop a liquefied shear strength relation.

9) The minimum $(N_1)_{60}$ blow count is used to develop $S_{U\text{-}LIQ}$ relations because flow failures are likely to develop along the "weakest-link". The second-order polynomial provides the highest R^2 value for the liquefied shear strength versus minimum $(N_1)_{60}$ relationship as compared to linear, exponential, logarithmic and power fits.

10) The R^2 value for the liquefied shear strength versus SPT blow count corrected using the Seed and Harder (1990) correction for fines content is higher than the Stark and Mesri (1992), and Youd et al. (2001) corrections.

11) The R^2 values for relationships developed for fines content corrected SPT blow counts are lower than R^2 values computed for relationships where the SPT blow counts are not corrected for fines content. The author's recommend use of the liquefied shear strength relationship shown in Figure 3-3 without a correction for fines content to estimate $S_{u\text{-}LIQ}$ from the minimum SPT blow count.

12) The liquefied shear strength should not be normalized by the initial vertical effective stress. It appears that insufficient information is available to provide a clear relationship between the minimum SPT blow count, the liquefied shear strength, and the initial vertical effective stress.

13) The yield shear strength is mobilized under the pre-failure geometrical conditions whereas the liquefied shear strength is mobilized under the post-failure geometrical conditions. The appropriate geometry should be used for calculations of the yield and liquefied shear strengths.

14) The slip surface corresponding to the minimum *FS* does not always correspond to the maximum P_F slip surface. The author's recommend using the minimum factor of safety surface to compute probabilities of failure for slopes and dams.

15) Spatial variability of soil deposits can be modeled with the exponential autocorrelation function. If the deterministic *FS* is less than 1, the P_F increases as the δ_0 decreases. Conversely, if the deterministic *FS* is greater than 1, the P_F decreases as δ_0 decreases. When the deterministic *FS* is equal to 1, δ_0 has no effect on the computed P_F. Therefore, the spatial variability of the liquefied shear strength does not affect the back-calculated $S_{u\text{-}LIQ}$ from flow failure case histories.

16) Several probabilistic procedures, including the First-Order Reliability Method and Monte Carlo Simulations can used in combination limit equilibrium methods to analyze case histories of flow failure such as those presented in Chapter 3.

17) The Beta probability density function is suitable for modeling all geotechnical parameters as the distribution can be truncated with minimum and maximum values. Estimates of parameter means and *COV* values can easily be represented with a Beta PDF.

18) Implementing a Bayesian Mapping procedure, values of P_F are computed from the probability density function of the reliability indices of flow failure. The mapping function is obtained relating the deterministic factor of safety to P_F for the deterministic liquefied shear strength relationship presented in Figure 4-1. The P_F can be computed using the BM equation and the deterministic factor of safety, computed with mean or average values.

19) Charts were developed based on BM of the case histories which provide several methods for screening soil slopes or dams containing liquefiable soils. The charts require two of three inputs for use, minimum $(N_1)_{60}$ blow count, flow failure demand *FFD*, or probability of flow P_F.

20) Without accounting for uncertainty in the performance function, probabilities of failure computed from the FORM or MCS may be inaccurate. It is shown that through an iterative procedure the mean and standard deviation of the model uncertainty term, C_1, can be estimated. The model uncertainty for the liquefied shear strength relationship presented in Figure 4-1 has a mean of 1.0 and standard deviation of 0.4, resulting in a *COV* of 40%.

21) The author's recommend performing probabilistic analyses with either the infinite slope model or Spencer's (1967) method of slices, depending on geometry, along with PDF's to model various input parameters.